

AD-A131 793

MAGNETOSPHERIC PLASMA STUDIES USING DATA FROM THE  
DYNAMICS HIGH AND LOW A. (U) SOUTHWEST RESEARCH INST  
SAN ANTONIO TX J N BARFIELD 15 MAY 83 SCIENTIFIC-1

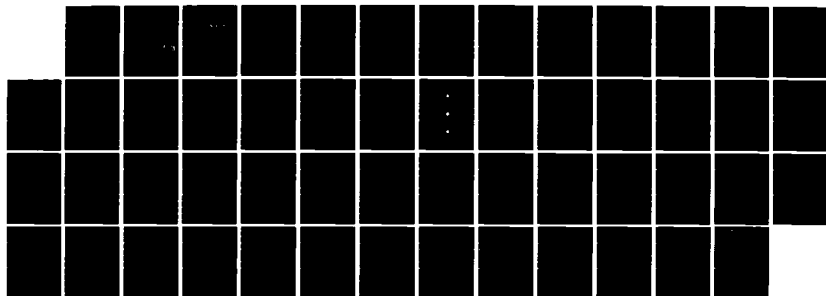
1/1

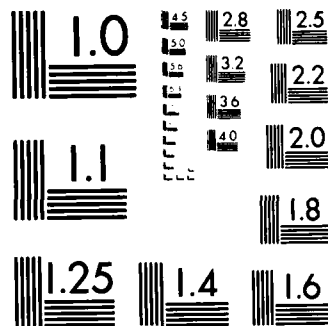
UNCLASSIFIED

AFGL-TR-83-0134 F19628-82-K-0024

F/G 4/1

NL





MICROCOPY RESOLUTION TEST CHART  
NATIONAL BUREAU OF STANDARDS 1963-A

ADA 131793

12

AFGL-TR-83-0134

MAGNETOSPHERIC PLASMA STUDIES USING DATA  
FROM THE DYNAMICS HIGH AND LOW ALTITUDE  
PLASMA INSTRUMENTS

J. N. Barfield

Southwest Research Institute  
P.O. Drawer 28510  
San Antonio, Texas 78284

Scientific Report No. 1

15 May 1983

DTIC  
ELECTE  
AUG 25 1983  
S A

Approved for public release; distribution unlimited

DTIC FILE COPY

AIR FORCE GEOPHYSICS LABORATORY  
AIR FORCE SYSTEMS COMMAND  
UNITED STATES AIR FORCE  
HANSCOM AFB, MASSACHUSETTS 01731

83 08 23 103

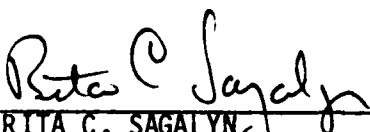
This report has been reviewed by the ESD Public Affairs Office (PA) and is releasable to the National Technical Information Service (NTIS).

This technical report has been reviewed and is approved for publication

  
\_\_\_\_\_  
ROGER P. VANCOUR  
Contract Manager

  
\_\_\_\_\_  
CHARLES P. PIKE  
Branch Chief

FOR THE COMMANDER

  
\_\_\_\_\_  
RITA C. SAGALYN  
Division Director

Qualified requestors may obtain additional copies from the Defense Technical Information Center. All others should apply to the National Technical Information Service.

If your address has changed, or if you wish to be removed from the mailing list, or if the addressee is no longer employed by your organization, please notify AFGL/DAA, Hanscom AFB, MA 01731. This will assist us in maintaining a current mailing list.

Do not return copies of this report unless contractual obligations or notices on a specific document requires that it be returned.

UNCLASSIFIED

SECURITY CLASSIFICATION OF THIS PAGE (When Data Entered)

REPORT DOCUMENTATION PAGE		READ INSTRUCTIONS BEFORE COMPLETING FORM
1. REPORT NUMBER AFGL-TR-83-0134	2. GOVT ACCESSION NO. 90 A13 1793	3. RECIPIENT'S CATALOG NUMBER
4. TITLE (and Subtitle) Magnetospheric Plasma Studies using Data from the Dynamics High and Low Altitude Plasma Instruments		5. TYPE OF REPORT & PERIOD COVERED Scientific Report No. 1
		6. PERFORMING ORG. REPORT NUMBER 15-7053-1
7. AUTHOR(s) J. N. Barfield		8. CONTRACT OR GRANT NUMBER(s) F19628-82-K-0024
9. PERFORMING ORGANIZATION NAME AND ADDRESS Southwest Research Institute P. O. Drawer 28510 San Antonio, TX 78284		10. PROGRAM ELEMENT, PROJECT, TASK AREA & WORK UNIT NUMBERS 62101F 766110AB
11. CONTROLLING OFFICE NAME AND ADDRESS Air Force Geophysics Laboratory Hanscom AFB, MA 01731 Contract Monitor: Roger Vancour/PHK		12. REPORT DATE 15 May 1983
		13. NUMBER OF PAGES 51
14. MONITORING AGENCY NAME & ADDRESS (if different from Controlling Office)		15. SECURITY CLASS. (of this report) UNCLASSIFIED
		15a. DECLASSIFICATION DOWNGRADING SCHEDULE
16. DISTRIBUTION STATEMENT (of this Report)  APPROVED FOR PUBLIC RELEASE; DISTRIBUTION UNLIMITED		
17. DISTRIBUTION STATEMENT (of the abstract entered in Block 20, if different from Report)		
18. SUPPLEMENTARY NOTES		
19. KEY WORDS (Continue on reverse side if necessary and identify by block number) Magnetosphere                      Space Plasma Ionosphere                          Environmental Specification Substorm                              Spacecraft Charging		
20. ABSTRACT (Continue on reverse side if necessary and identify by block number) Plasma data from the High and Low Altitude Plasma Instruments aboard the Dynamics 1 and 2 (DE-1 and DE-2) satellites have been analyzed to investigate high latitude plasma characteristics. DE-1 hot plasma observations in the mid-altitude polar cusp have shown evidence of a significant velocity filtering phenomenon which is consistent with a latitudinally narrow region of plasma injection located at a geocentric distance of about 8 earth radii (RE). This velocity filtering effect allows the measurement of much smaller flow velocities (about 10 km/s) than have heretofore been possible.		

DD FORM 1 JAN 73 1473

UNCLASSIFIED

SECURITY CLASSIFICATION OF THIS PAGE (When Data Entered)

UNCLASSIFIED

SECURITY CLASSIFICATION OF THIS PAGE(When Data Entered)

with plasma measurements. Observations at altitudes of 2-3 RE indicate two distinct types of counterstreaming electron events. The type 1 event is characterized by two Maxwellian distribution functions, an isotropic high-temperature component and a field-aligned low temperature component. Type 1 events appear to involve wave-particle interactions while type 2 events imply direct acceleration by oppositely-directed electric fields pointing toward the satellite along magnetic field lines. Conjunctive observations of the DE-1 and DE-2 satellites and a scanning photometer on the ground have allowed the identification of the low energy, heated electron population associated with 6300A SAR ARC emission. Analysis of a SAR ARC observed on day 296 of 1981 shows the electrons to be fairly Maxwellian with temperatures on the order of  $9900 \pm 1100^\circ\text{K}$  and an earthward field-aligned velocity of approximately  $275 \pm 60 \text{ km/s}$ . The electrons are not accompanied by precipitation. The ion loss cone is empty at least as high as 6000 km. Measurements on DE-1 have shown that intense upward electron beams with energies from about 20 electron volts to about 200 electron volts are a common feature of the region equatorward of the morning-side polar cusp. Computations of the currents carried by these beams and by the precipitating cusp electrons show excellent agreement with the simultaneous DE-1 magnetometer measurement for both upward and downward Birkeland currents. The data indicate that cold ionospheric electrons, which carry the downward region-1 Birkeland currents on the morning side, are accelerated upward by potential drops of tens of eV at altitudes of several thousand kilometers. This acceleration process allows spacecraft above those altitudes to measure routinely the charge carriers of both downward and upward current systems.

UNCLASSIFIED

SECURITY CLASSIFICATION OF THIS PAGE(When Data Entered)

# TABLE OF CONTENTS

	<u>PAGE</u>
I. INTRODUCTION	1
II. PLASMA INJECTION AND TRANSPORT IN THE MID-ALTITUDE POLAR CUSP	2
III. OBSERVATIONS OF COUNTERSTREAMING ELECTRONS AT HIGH ALTITUDES	10
A. Type 1 Counterstreaming Electrons	11
B. Type 2 Counterstreaming Electrons	14
C. Conclusions	20
IV. UPWARD ELECTRON BEAMS	21
A. Introduction and Observations	21
B. Electron Currents and Magnetic Perturbations	24
C. Acceleration Mechanism	25
D. Conclusions	28
V. OBSERVATIONS OF A HEATED ELECTRON POPULATION ASSOCIATED WITH THE 6300 Å SAR ARC EMISSION	30
A. Introduction and Observations	30
B. Discussion	33
C. Summary	38
VI. PRESENT STATUS AND FUTURE STUDIES	39
REFERENCES	40
PAPERS PRESENTED AT SCIENTIFIC MEETINGS	44
PUBLICATIONS SUPPORTED BY CONTRACT	46
PERSONNEL	47

Accession For	
NTIS GRA&I	<input checked="" type="checkbox"/>
DTIC TAB	<input type="checkbox"/>
Unannounced	<input type="checkbox"/>
Justification	
By	
Distribution/	
Availability Codes	
Dist	Special
7	

## I. INTRODUCTION

Research performed during the first year of this contract focussed primarily upon plasma processes in and near the polar cusp, and upon establishment of the statistical data base from which a specification of the polar cap plasma environment will be produced.

Four basic areas will be covered in this report: Plasma injection and transport in the mid-altitude polar cusp; observations of counterstreaming electrons at high altitudes; observations of upward electron beams and their relationship to Region-1 Birkeland currents; and observations of the electron population responsible for the 6300A SAR arc emission.

The primary observing platform for the research reported here was Dynamics Explorer 1 (DE-1). The DE-1 High Altitude Plasma Instrument (HAPI) consists of five electrostatic analyzers mounted in a fan-shaped angular array at angles of 45°, 78°, 90°, 102°, and 135° with respect to the spacecraft spin axis. Each analyzer makes differential measurements of electrons and positive ions over an energy/charge range of 5 eV/e to 32 keV/e. Energy stepping proceeds at commandable rates of up to 64 sec<sup>-1</sup>, providing three-dimensional plasma distribution functions at the six-second spin rate of DE-1 (Burch et al., 1981).



## II. PLASMA INJECTION AND TRANSPORT IN THE MID-ALTITUDE POLAR CUSP

Ion fluxes in the cusp often show a "dispersion" signature, in which the characteristic ion energy falls with increasing latitude (Shelley et al., 1976; Reiff et al, 1977). The dispersion signature occurs because poleward ( $\bar{E} \times \bar{B}$ ) convection acts as a "velocity filter" on the incoming plasma. Particles with large parallel velocities arrive at the earth sooner (therefore, more equatorward) than particles with lower parallel velocities. Pitch angle effects on the velocity dispersion are not important at low altitudes (Reiff et al, 1977). This is not the case in the mid-altitude cusp (Frank, 1971; Gurnett and Frank, 1978), where the transit time from injection to observation of a particle of a given energy is a strong function of pitch angle. This fact enables us to obtain independent measurements of the injection altitude for each spin of the DE-1 satellite and to determine local flow velocities as low as  $\sim 10$  km/s.

On a typical polar-cusp pass, as the satellite enters the cusp, ion fluxes first appear in higher ( $\sim 1-3$  keV) energy channels clustered about  $0^\circ$  (downward) pitch angles ( $\alpha$ ). Then the energy of peak ion energy flux decreases systematically and the distribution spreads to larger pitch angles in a distinctive 'V' pattern, in which the peak energy flux occurs at higher energies for larger pitch angles. As this pattern continues to evolve, the 'V' signatures deepen to reach energies near 200 eV at  $0^\circ$  and spread through all downward pitch angles and a wide range of upward pitch angles. Eventually, strong ion fluxes are observed at all pitch angles except for the narrow loss cone ( $\sim 7^\circ$ ) around  $\alpha = 180^\circ$ . Finally, a dropout develops at  $\alpha \sim 0^\circ$  and spreads through all downward pitch angles so that only upward moving ions, which have mirrored below the spacecraft, are observed.

We have attempted to explain the ion energy/pitch-angle signatures observed by DE-1 in the mid-altitude cusp by application of a simple plasma-injection model in which cusp field lines are convected through a spatially restricted region of plasma injection and then into the polar cap. In a dipole magnetic field the guiding center approximation is used to compute an  $E(\alpha, t)$  relationship for particles observed at a nominal geocentric distance of  $4 R_E$  and a dipole invariant latitude of  $78^\circ$ . The relationship has the following form:

$$E(\alpha_0, t) = \frac{M}{2t^2} \left[ \int_{s_i}^{s_o} \frac{ds}{1 - \sin^2 \alpha_0 \left( \frac{B(s)}{B_0} \right)} \right]^2, \quad (1)$$

where,

$ds$  is arc length along a dipole field line,

$s_o, s_i$  are the observation and injection points,

$M$  is the particle mass,

$B(s)$  is the magnetic induction along the field line,

$B_0$  is the magnetic induction at the observation point,

$\alpha_0$  is the observed pitch angle,

$t$  is the transit time.

For  $\alpha_0 > 90^\circ$ , the integration is carried down to the mirror altitude and back up the field line to the observation altitude.

Since  $M$  and  $t$  appear only in the factor  $\frac{M}{2t^2}$  in eq. (1), the shape of the  $\log E$  vs.  $\alpha_0$  curve for given injection and observation points will be independent of transit time and will be applicable to ions of all masses as well as

to electrons. Computed  $\log E$  vs.  $\alpha_0$  curves are plotted in Fig. 1 for injection radii of  $6 R_E$ ,  $8 R_E$ ,  $12 R_E$ , and  $16 R_E$ , and an observation radius of  $4 R_E$ . For ease of comparison the four curves are adjusted to coincide at  $\alpha_0 = 90^\circ$ . Also plotted in Fig. 1 are the DE observations for a single spin covering the time period from 14:07:30 to 14:07:36 on September 29, 1981. The data points in Fig. 1 are strongly indicative of an injection distance in the neighborhood of  $8 R_E$  (geocentric). Injection distances beyond  $12 R_E$  would clearly not result in the strong  $(E, \alpha_0)$  dependence that is observed at  $\sim 4 R_E$  by DE-1.

As the observation point moves to lower altitudes, the model predicts that the  $\log E$  vs.  $\alpha_0$  dependence will rapidly become weaker, causing the disappearance of any significant 'V' shape at, for example, the typical DE-2 altitude of 900 km. This prediction is borne out by the DE-2 observations and by the fact that no other low-altitude spacecraft or sounding rockets have observed the 'V' shaped  $\log E$  vs.  $\alpha_0$  relationship.

Fig. 2 displays the computed time evolution of the  $\log E$  vs.  $\alpha_0$  relationship for  $H^+$  with an injection point at  $8 R_E$  and an observation point at  $4 R_E$ . All the curves in Fig. 2 have the same shape, with the vertical position of each curve determined only by the relationship  $vt = \text{constant}$ . The energy scale in Fig. 2 is arbitrarily truncated at just over 3 keV and at 100 eV to coincide approximately with the high and low energy limits of the observed ion fluxes. Fig. 2 then allows one to trace the  $\log E$  vs.  $\alpha_0$  relationship as a function of elapsed time after injection for an input  $H^+$  spectrum that falls off rapidly at energies above 3 keV and below 100 eV. For heavier ions the elapsed times in Fig. 3 would be multiplied by  $\sqrt{M/MH^+}$ ; for electrons the times would be smaller by a factor of 43.

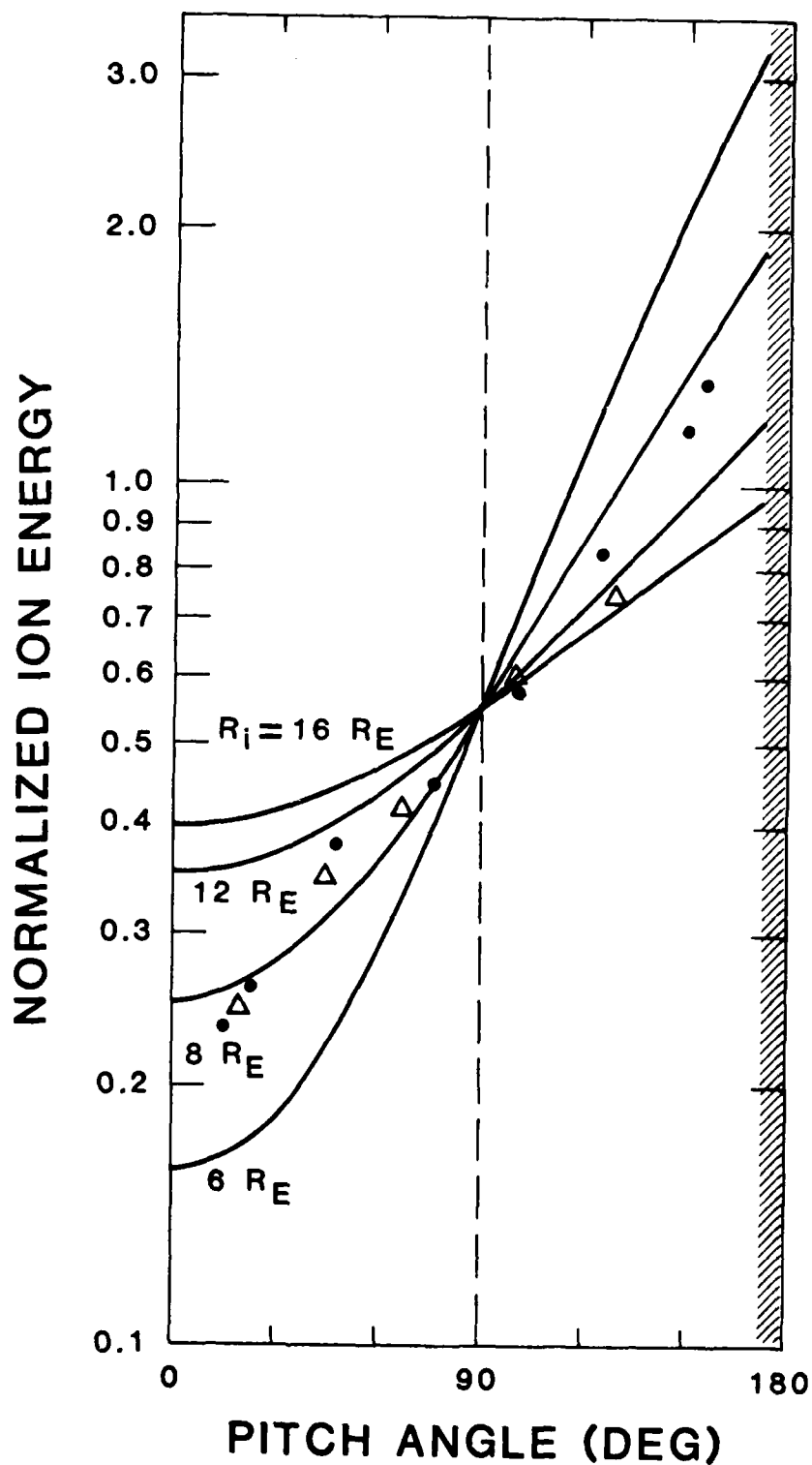


Figure 1. Computer energy/pitch-angle relationship for particles injected at geocentric radial distance  $R_i$  on the  $78^\circ$  dipole magnetic field line and observed at a later time at a distance of  $4 R_E$  on the same field line. The shaded region is the 400 km loss cone. Data points denote the energy of peak ion energy flux observed during one full spin of DE-1 (dots for  $0^\circ$  to  $180^\circ$  and triangles for  $180^\circ$  to  $0^\circ$ ).

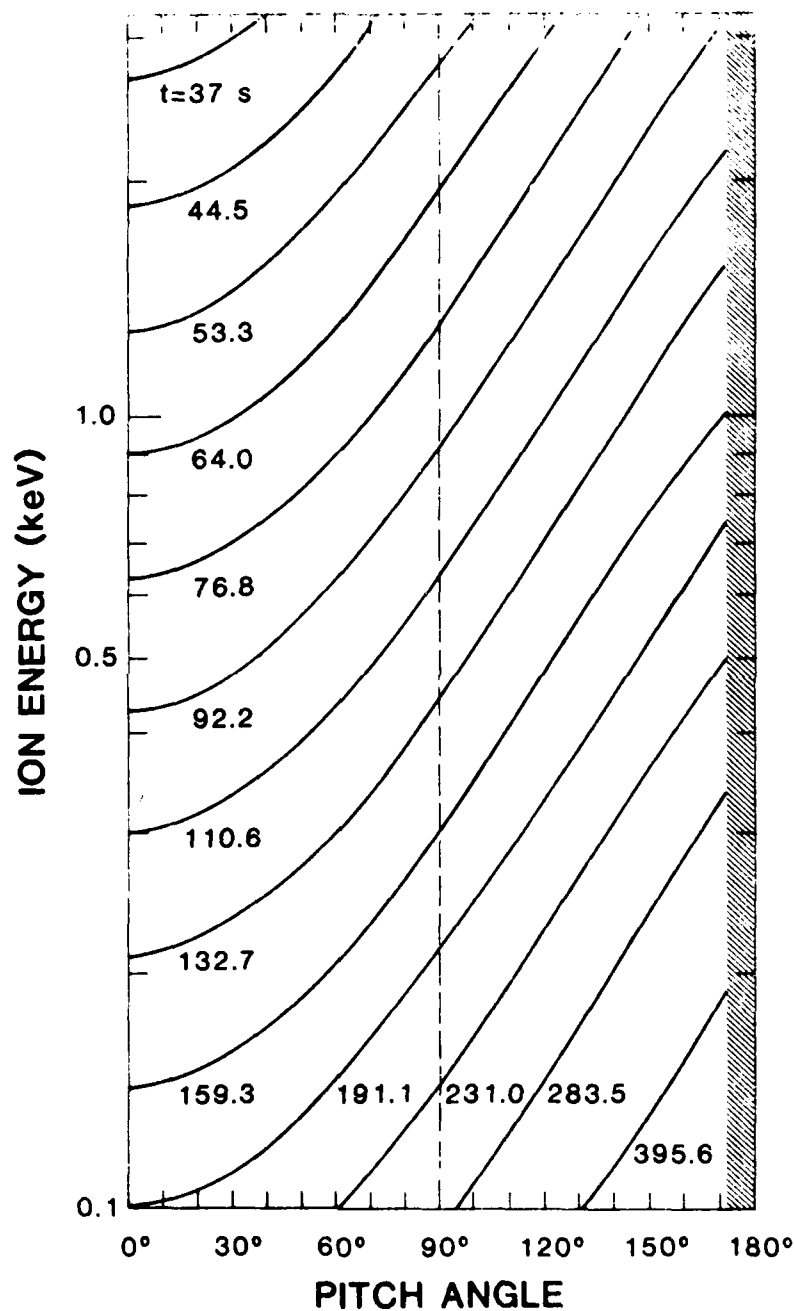


Figure 2. Temporal development of computed energy/pitch angle relationship for  $H^+$  ions injected at  $R_i = 8 R_E$  and observed at  $R = 4 R_E$ .

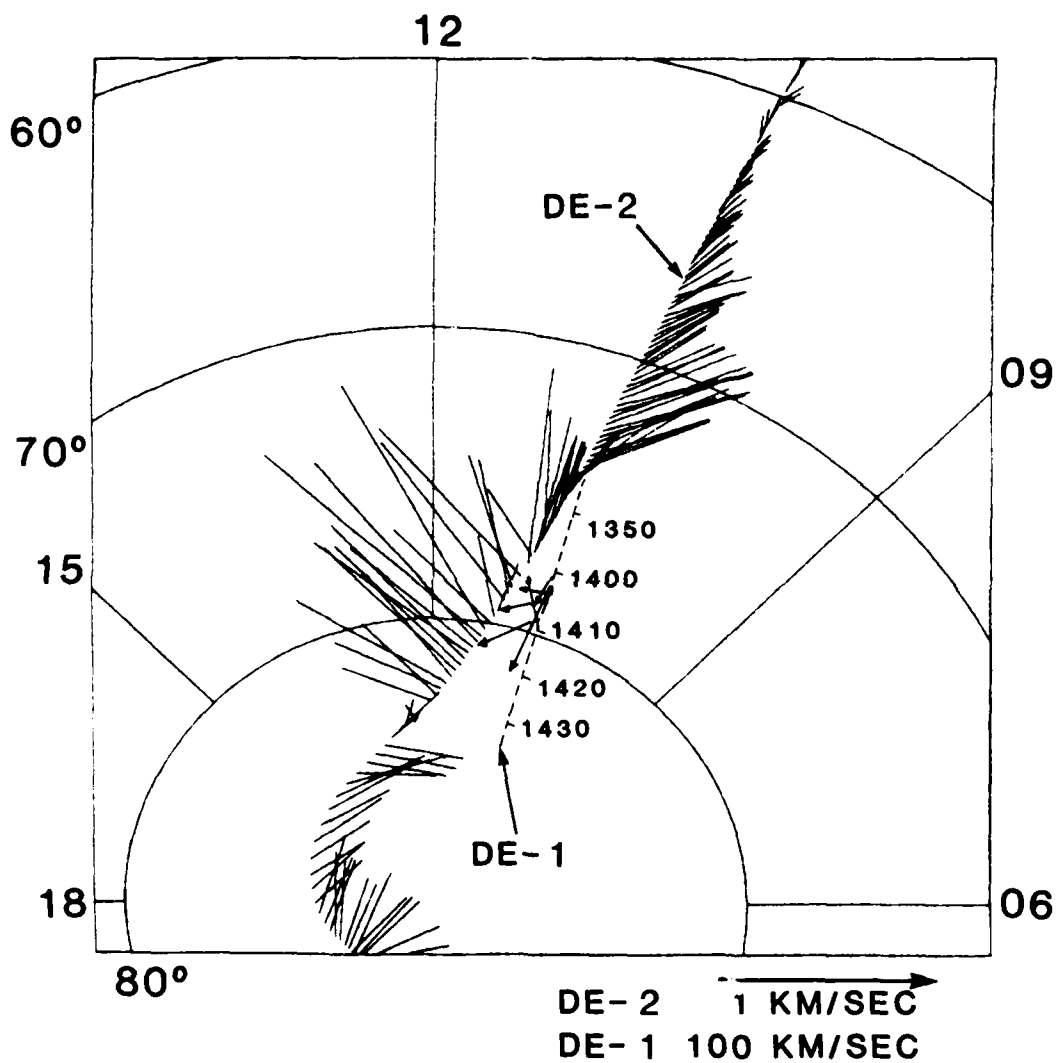


Figure 3.  $\Lambda$ -MLT plot of ion flow vectors measured nearly simultaneously at ~19,000 km (DE-1) and ~500 km altitude (DE-2) on September 29, 1981. At 14:06 UT DE-2 was moving poleward at  $\Lambda = 78.7^\circ$  and MLT = 11.14 hr. UT in hours and minutes is noted along the DE-1 orbital track.

The time evolution of the  $\log E$  vs.  $\alpha_0$  curves could result from the convection of cusp field lines through a restricted region of plasma injection or from a single impulsive injection event over the entire cusp. However, in the latter case, unless cusp ion injection is very infrequent (several minutes between injections) several of the curves of Fig. 2 would exist simultaneously, and the distinct 'V'-shaped  $E, \alpha_0$  signature would not appear. Time-dependent injection no doubt occurs (Carlson and Torbert, 1980) but, to be consistent with DE-1 data, must be confined to a restricted injection region located near the low-latitude edge of the cusp.

The cusp velocity filter effect allows us to observe a specific velocity at each pitch angle. The velocity selected by the filter is gyrotropic, i.e., independent of gyrophase angle, if one is in the rest frame of the magnetic field line. If the field line is convecting past the spacecraft, the convection velocity adds vectorially to the velocity selected by the filter effect. Since each detector observes  $90^\circ$  pitch-angle particles twice per spacecraft spin, one can construct a particle phase-space distribution for the plane perpendicular to the magnetic field direction, and have ten independent look directions in that plane. Each look direction will show the velocity filter effect, with a peak distribution function at a specific velocity within the uncertainty due to the logarithmic spacing of the energy steps. We can then fit an offset circle to the velocity of the peak distribution function. The magnitude of the offset gives us the locally measured flow velocity, and the direction of the offset yields the direction from which the plasma is flowing. The flow velocities determined in this way at DE-1 are plotted along with concurrent DE-2 flow measurements (Heelis et al. 1981) in Fig. 2 for a typical cusp pass. The agreement between the two flow patterns is fairly good, considering the difficulty and uncertainty in the high-altitude measurement.

The magnitude of flows in a dipole field geometry should map upward along field lines approximately as  $r^{3/2}$ . The flow velocities at DE-1 should, therefore, be roughly six times as high as at DE-2. Fig. 3 shows that the measured flow velocities are more nearly 15 to 20 times the DE-2 flows. Possible reasons for the apparent enhancement of flow velocities at higher altitudes will be the subject of further study.

The cusp plasma injection model presented above predicts that the shape of the  $\log E$  vs.  $\alpha_0$  curves should be the same for ions and electrons if the altitudes of injection and observation are equal. However, the progression of the curve down the energy axis of Fig. 2 will proceed 43 times as fast for electrons as for  $H^+$ . Since cusp electron energies are generally between 10 eV and 200 eV, Fig. 2 shows that the entire progression will take place during a time interval between about 5 seconds and 20 seconds following injection. In the continuous injection model this prediction means that for the 'V'-shaped signatures to be observed in the electrons, the spacecraft must cross a field line within about 10 seconds of the time it convected out of the injection region. However, there are times when electron 'V's are observed. As expected, the 'V' signatures are observed in only one or two spacecraft spin periods just adjacent to the cusp equatorward electron boundary. The ion 'V's are observed to be displaced poleward from the electron 'V's, again as expected from the simple model of a spatially restricted injection region from which cusp plasma is convected into the polar cap.



### III. OBSERVATIONS OF COUNTERSTREAMING ELECTRONS AT HIGH ALTITUDES

Counterstreaming electrons have been observed by the High-Altitude Plasma Instrument (HAPI) on the DE-1 satellite. Previously, counterstreaming electrons have been detected by the S3-3 satellite as narrowly collimated beams of electrons with energies around one keV streaming both parallel and antiparallel to the magnetic field direction (Sharp et al., 1980). The S3-3 observations were made at altitudes between 4000 and 8000 km, while the present work pertains to observations of phenomena at higher altitudes ( $\approx 2 R_E$ ).

Some features of counterstreaming electrons suggest that the mechanism responsible for electron acceleration is not associated with quasi-static electric fields (Sharp et al., 1980). For example, counterstreaming electrons have broad and unstructured energy spectra that can be fitted by Maxwellian functions with temperatures varying from 0.5 to 1 keV. Simultaneous measurements of conic ions of  $H^+$  and  $O^+$  in the pitch angle range of  $90^\circ$  to  $125^\circ$  during counterstreaming electron events also support the suggestion that a quasi-static electric field is not necessarily involved. However, the S3-3 satellite has occasionally detected peaks in the energy spectra of counterstreaming electrons.

Our preliminary survey of DE-1 HAPI data indicates that there are two distinct types of counterstreaming electron events. The first type of event is fairly stable and has broad and unstructured energy spectra not suggestive of acceleration by parallel electric fields. The second type is transient, and has beam-like distribution functions, which are consistent with acceleration by parallel electric fields. The first type is found to be similar to those frequently observed by the S3-3 satellite, while the presence of the second

type is only hinted at in the S3-3 observations. These two types of events become quite distinguishable in the HAPI data because DE-1 has a faster spinning rate and the HAPI instrument is able to obtain the plasma distribution function at a higher time resolution as compared to the previous observations. We shall examine these two types of events separately and refer to them as type 1 and type 2 counterstreaming electron events respectively.

#### A. Type 1 Counterstreaming Electrons

A typical example of the electron distribution functions parallel and anti-parallel to the field direction measured during a Type 1 counterstreaming event is presented in Figure 4 (with X symbols). An electron distribution function during one counterstreaming electron event observed by the S3-3 is deduced from Sharp et al (1980) and presented here for comparison (with triangle symbols). Except for a difference in the magnitude, these two distribution functions are very similar, as both can be approximated by a superposition of two Maxwellian functions. The temperature of the counterstreaming component is estimated to be about 200 eV, while the high energy isotropic component is estimated to have a temperature of about 1.5 keV. It appears that this type of event is related to the counterstreaming electron events reported by Sharp et al (1980).

The pitch angle range of counterstreaming electrons observed is about  $30^\circ$ , much wider than the local loss cone ( $\approx 13^\circ$ ). The counterstreaming electron component is found to extend to larger pitch angles with smaller density; this might be considered as evidence of pitch angle scattering.

Figure 4 indicates that the distribution function of counterstreaming electrons is higher in the downward direction ( $18^\circ < \alpha < 30^\circ$ ) than in the upward

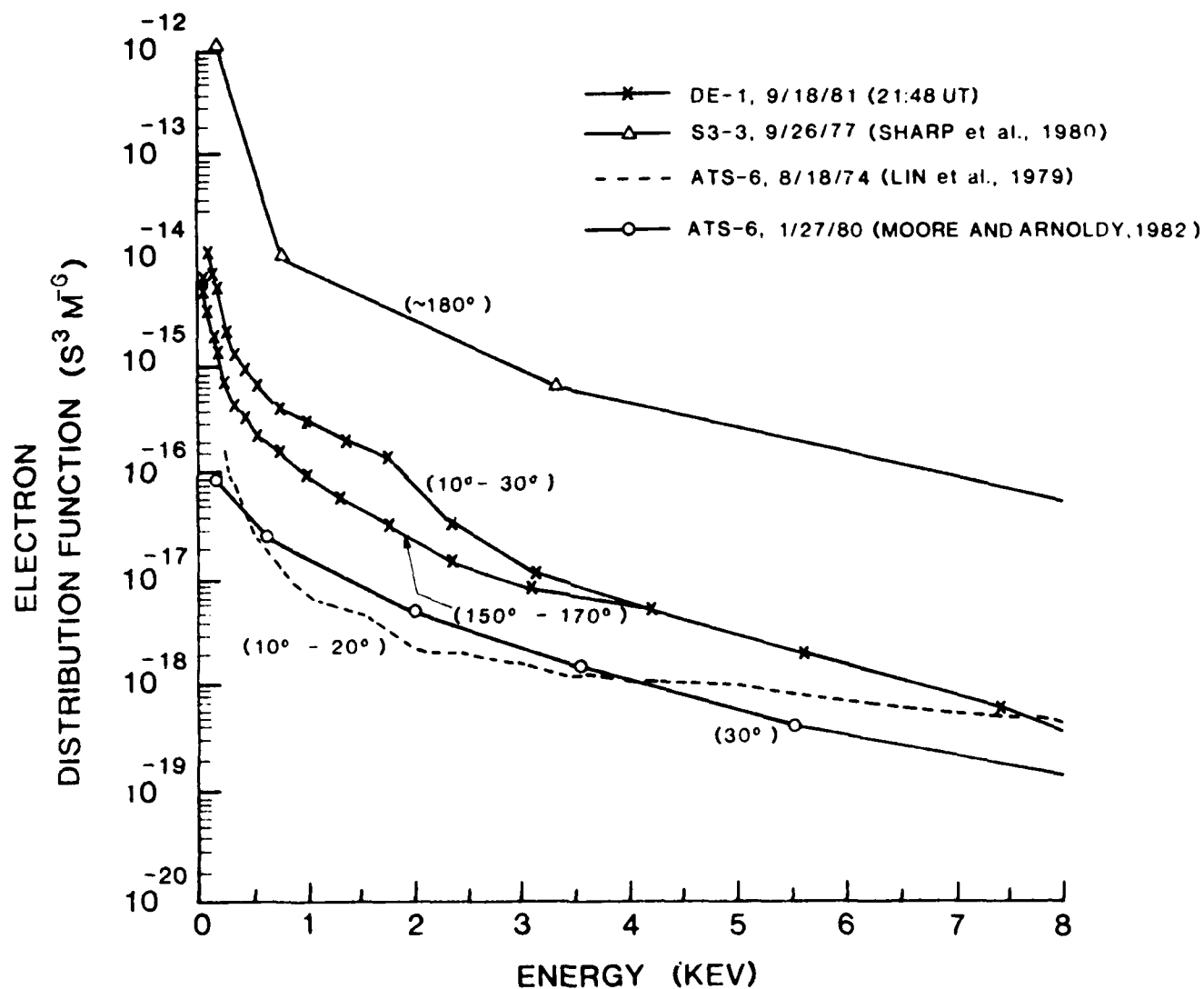


Figure 4. Electron distribution function of type 1 counterstreaming electrons (measured by DE-1 and S3-3) and field-aligned electron beam (measured by ATS-6).

direction ( $150^\circ < \alpha < 170^\circ$ ), more specifically, about four times higher at energies less than 2 keV. For this particular event, we found the downward enhancement to be about 2 for most times with an occasional enhancement in the opposite direction.

One type of counterstreaming electron frequently detected by the DE-1 HAPI instrument is an enhancement of field-aligned electron fluxes in both upward and downward directions. These counterstreaming electrons can be characterized by a Maxwellian distribution function with a temperature of about 200 eV. Their occurrence seems to be associated with isotropic precipitation of electrons with energies greater than 1 keV.

In Figure 4 we have also plotted two electron distribution functions of field-aligned electron beams measured by ATS-6 on the equatorial plane during substorm injection events (Lin et al., 1979; Moore and Arnoldy, 1982). It is interesting to notice that they are characterized by two Maxwellian functions as well. The magnetograms at local midnight are not available yet to learn if type 1 counterstreaming electrons occur during substorm injections, but the Kp magnetic activity index was certainly high (6-) for this event. It is possible that counterstreaming electrons and substorm injected electron beams are related.

A simple interpretation of type 1 counterstreaming electrons is that these electrons are produced at the topside ionosphere as thermal electrons heated to higher temperature through wave-particle interactions. The heated electrons appear as streaming particles as they move up along field lines. In order to explain the counterstreaming feature, the heating should take place continuously for long duration above both ionospheres. However, this interpretation does not explain the events described by Sharp et al (1980) which were much narrower than the loss cone.

Another possible interpretation is that type 1 counterstreaming electrons are secondary electrons produced by collisions of precipitating electrons with the atmosphere, as suggested for substorm-injected electron beams by Moore and Arnoldy (1982). Wave particle interactions then cause the electrons to be scattered outside the loss cone. The diffusion coefficient  $D$  can be estimated according to  $(\Delta\alpha)^2/2\Delta t$ , where  $\Delta\alpha$  is the average pitch angle change and  $\Delta t$  is the interaction time. We estimate  $\Delta\alpha$  to be about  $12^\circ$  and  $\Delta t$  to be the elapsed time for electrons of 500 eV to travel from the topside ionospheres to the satellite. We find  $D$  to be about  $9 \times 10^{-3} \text{ sec}^{-1}$  for electrons originating from the northern hemisphere and  $3 \times 10^{-3} \text{ sec}^{-1}$  for electrons originating from the southern hemisphere. The estimated  $D$ , which represents an upper limit, agrees in order of magnitude with the diffusion rate estimated for substorm-injected electron beams (Lin et al., 1979; Moore and Arnoldy, 1982).

We notice that the electron distribution function observed by the S3-3 is about one order of magnitude larger than the DE-1 measurement. This difference could be attributed to different events or instrumental effects. This difference might also be interpreted as an altitude dependence since the S3-3 altitude was much lower than the DE-1 altitude.

#### B. Type 2 Counterstreaming Electrons

Contours of the logarithm of the electron distribution function are plotted in Figure 5 for three 6-second time intervals during a type 2 event: (a) before, (b) during and (c) after the counterstreaming electron event. In the figure, solid lines of circles and hyperbolas are theoretical predictions of the separation boundary between ionospheric and magnetospheric populations when a quasi-static electric field is assumed above and below the satellite (Chiu and Schulz, 1978; Mizera et al., 1981). Following Mizera et al. (1981),

## DE-1 HAPI ELECTRON DISTRIBUTION CONTOURS

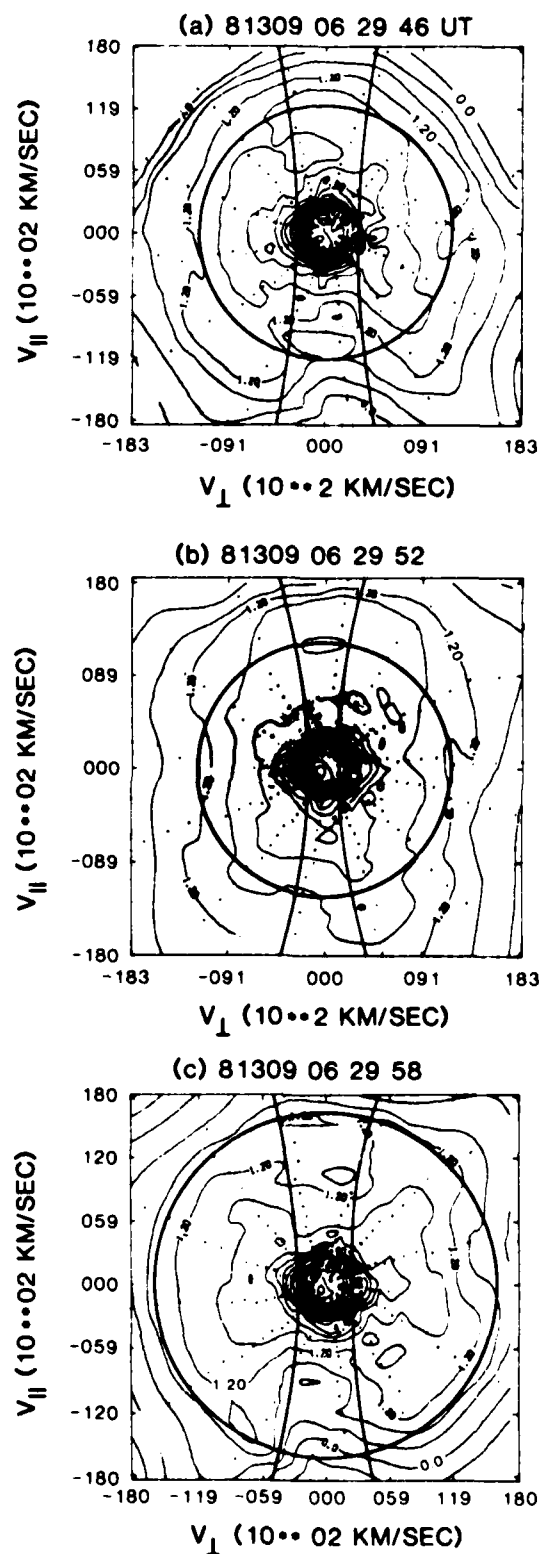


Figure 5. Electron phase space density contours (a) before, (b) during and (c) after a type 2 counterstreaming electron event.

we infer the potential drop below the satellite to be the ion beam energy and the potential drop above the satellite to be the electron beam energy. The electron and ion beam energies are determined from the plot of the distribution function along the  $V_{\parallel}$  axis. The computed demarcation curves appear to characterize reasonably the phase space density contours before and after, but not during the event. More specifically, the hyperbolas in Figures 5a and 5c mark well the electron loss cone and the low energy core of presumably ionospheric electrons. Figures 5a and 5c indicate a slight enhancement of phase space density in the forbidden region between the circle and the hyperbola. These features resemble the S3-3 observations of electron phase space density contours during electrostatic shocks (e.g. see a review by Fennell et al., 1981). In contrast, the hyperbola in Figure 5b lies well inside the region of the low energy core. Furthermore, Figure 5b displays a distinct counterstreaming feature, an electron beam at an energy of 416 eV ( $v_{\parallel} = 12000$  km/sec) along the  $+v_{\parallel}$  axis and a weak electron beam at an energy of about 100 eV ( $v_{\parallel} = -5920$  km/sec) along the  $-v_{\parallel}$  axis. The phase space density contours show no loss cone feature and are very elongated along the  $v_{\parallel}$  axis up to about  $v_{\parallel} = 15000$  km/sec (or 800 eV). Figure 5b therefore cannot be explained by a simple potential drop that increases monotonically from the magnetosphere to the ionosphere.

The type 2 counterstreaming electron event is distinguished from type 1 events in several respects. First of all, the electron distribution function has a beam-like structure. Second, the electron energy flux lacks a hot component ( $>1$  keV). Finally, the ion energy fluxes observed during the type 2 event have pitch angles near  $175^{\circ}$ , much closer to the magnetic field direction than those of the conic ions detected in the type 1 events. The type 2 event may

have been observed by the S3-3 satellite, since S3-3 occasionally detects energy spectra with beams during counterstreaming electron events (Sharp et al., 1980).

One unusual feature of type 2 counterstreaming electrons is the elongation of the phase density contours along the  $v_{\parallel}$  axis (see Fig. 5b). The elongated contours can be interpreted as electron beams reflected by a potential barrier. The HAPI measurement therefore suggests an upward electric field above the satellite and a downward electric field below the satellite. To produce such an oppositely-directed electric field, we suggest V-shaped potential contours imbedded with a potential island (valley). A schematic illustration is given in Fig. 6. This potential profile could explain the decrease of ion beam energy if the satellite passed through the transition region between the potential island and the V-shaped potential as shown in Fig. 6.

Sharp et al (1980) suggested another interpretation of counterstreaming electrons in terms of a double layer with a potential drop of about 1 keV flickering its polarity about every 1 millisecond. To account for the HAPI observation, we estimate the flickering period to be at least 50 milliseconds since the counterstreaming portion of the electron spectra was detected successively for three energy steps. Low altitude satellite observations of auroral particle fluxes have not yet suggested flickering double layers of such long periods.

The observed sequence of the type 2 event presented in Figure 5 could be interpreted either as a spacecraft horizontally crossing a V-shaped potential structure or as a vertical motion of the structure passing the spacecraft along magnetic field lines toward the ionosphere. If DE-1 were detecting a spatial structure, the transverse width of the potential island could be as



narrow as 16 km along the satellite path which corresponds to a North-South distance of about 1 km at the ionosphere. On the other hand, if DE-1 were detecting temporal variations, the potential island would be very transient, lasting only about one satellite spin period.

Potential contours with an island structure have recently been found in a computer simulation of two-dimensional double layers in which the effects of magnetic mirror force, trapped electrons and background plasmas are included (Wagner, 1980; Wagner et al., 1981). Recent laboratory experiments on double layers also indicate a similar structure (Iizuka et al., 1982). The condition for producing such a potential structure is not clear, although computer simulations by Wagner (1980) suggest strong wave trapping due to the Buneman instability. We notice that the potential profile in Figure 6 is very similar to the magnetic field and electric potential overshoots of the earth's bow shock which arise from reflections of a portion of the solar wind ion population (Russell and Greenstadt, 1979; Leroy et al., 1981). This analogy might be applied to the present case if we speculate that the potential well in Figure 6 is caused by reflection of ionospheric electrons.

Finally, we note that the width of the loss cone shown in Figures 5a and 5c is energy dependent (about 33° at 738 eV and about 40° at 416 eV). These loss cone widths are found to agree with the presence of a potential drop below the spacecraft according to the formula (Sharp et al., 1979)

$$\alpha = \sin^{-1} (B_g (E + eV) / B_i E)^{1/2} \quad (2)$$

where  $E$  is the energy,  $eV$  is the potential,  $B_g$  and  $B_i$  are the magnitudes of the magnetic field at the locations of the satellite and the top of the ionosphere respectively.

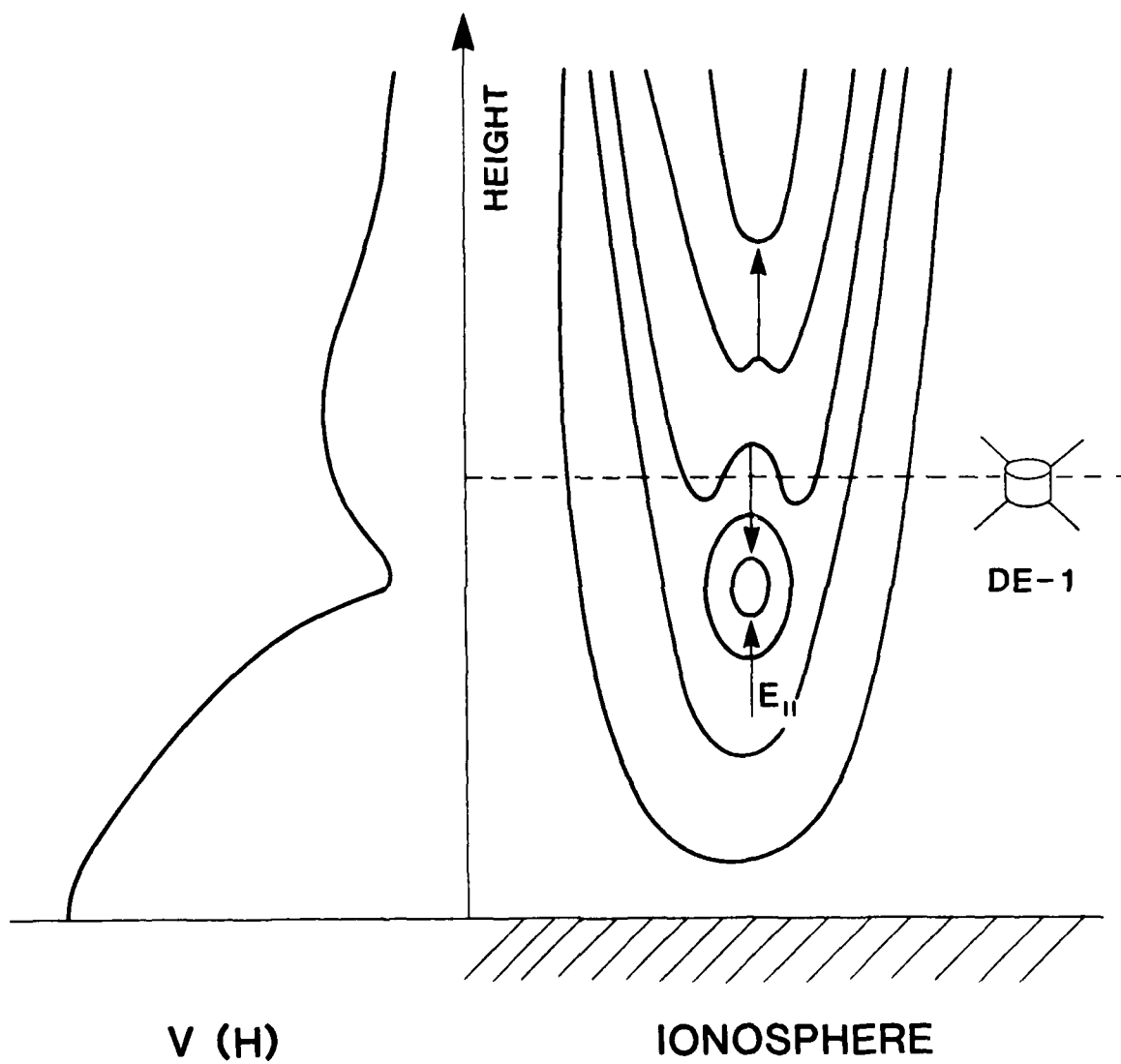


Figure 6. Schematics of V-shaped potential contours with a potential island.

### C. Conclusions

Type 1 counterstreaming electrons are apparently the type of electron event first reported by Sharp et al. (1980), and may be related to the field-aligned electron beams observed by the ATS-6 satellite at synchronous orbit during substorm injections (Lin et al., 1979; Moore and Arnoldy, 1982). Type 2 counterstreaming electrons are a new and unusual phenomenon that DE-1 has detected within acceleration regions. The main feature distinguishing these two types of event is that the electron distribution function of type 1 is composed of two Maxwellian distributions while the distribution function of type 2 is characterized by electron beams.

The presence of two distinct types of counterstreaming electron events indicates the possibility of two distinct mechanisms of electron acceleration operative at high altitudes in the auroral zone. Type 1 events appear to involve wave-particle interactions whereas type 2 events seem to result from direct acceleration by oppositely-directed electric fields pointing toward the satellite along magnetic field lines.

#### IV. UPWARD ELECTRON BEAMS

##### A. Introduction and Observations

The carriers of the large-scale Birkeland currents linking the ionosphere and the magnetosphere have typically been thought to be upward-moving thermal electrons in the downward-current regions and precipitating auroral electrons in the upward-current regions (Anderson and Vondrak, 1975; Klumpar, 1979). However, the problem is complex, and both populations can coexist in regions of upward or downward net current. For example, in the duskside plasma sheet where the current is typically downward, the upward flux of cold ionospheric electrons must be larger than that inferred from in situ magnetometer measurements, since it must also balance the upward current caused by the precipitation of energetic electrons. Similarly, intense auroral electron precipitation is often accompanied by upward fluxes of near-thermal and low-energy (<50 eV) electrons whose current can balance roughly half of the primary upward current (Maier et al, 1980). These low-energy electrons are probably secondaries produced by the auroral beam itself (Evans, 1974; Pulliam et al, 1980).

Narrowly-collimated electron beams also can contribute significantly to the total current balance. Unlike the substantially isotropic auroral electron precipitation, downward beams are often seen at the edges of auroral arcs (Anderson, 1979), at energies below the parallel potential drop within "inverted V's" (Burch et al, 1979; Lin and Hoffman, 1979) and in the cusp (Zanetti et al, 1981). Upward-flowing and counter-streaming electron beams have recently been observed by Lin et al (1982) and by Sharp et al (1980). Sharp et al attributed their S3-3 results to fluctuating double layers, and reported

that the width in pitch angle of the upward electron beams increases with increasing electron energy. We have found that this property is a consequence of a parallel potential drop below the spacecraft and that the amount of spread is related to the altitude of the top of the potential drop.

Similar upward electron beams were reported at lower ( $\sim 1400$  km) altitudes by Johnstone and Winningham (1982) and by Klumpar and Heikkila (1982). The latter study showed that the upward beams were imbedded in a much larger region of downward Birkeland current. Using S3-3 data, Collin et al (1982) showed that the occurrence frequency of upward beams is roughly eight times higher above 6000 km than below 3000 km. Thus, one can infer a sporadic low-altitude mechanism and a more stable mechanism near  $1 R_E$ .

The DE-1 spacecraft is an ideal platform from which to study these phenomena for three reasons: (1) The spacecraft moves slowly enough through the acceleration regions that spin aliasing is not a problem, as it was in the Maier et al and Klumpar and Heikkila studies; (2) The apogee ( $\sim 5 R_E$  geocentric) is high enough that effects from both the low-altitude and  $\sim 1 R_E$  acceleration regions can be observed, as well as any regions in the  $1-4 R_E$  altitude range; and (3) the presence of upward electron acceleration mechanisms below the DE-1 altitude brings the cold ionospheric electrons that carry the downward current at low altitudes up into the suprathermal energy range where they can readily be detected.

Upward electron beams have been observed at altitudes above 15,000 km on DE-1. These observations were made primarily near the equatorward edge of the dawnside polar cusp (statistically a locus of downward current) and sporadically throughout the cusp region. Upward electron beams are seen all through the region of downward current, and the magnitude of the currents carried by the 15 eV to 17 keV electrons are more than adequate to represent

east-west magnetic perturbations measured concurrently in both the upward and downward current regions. The beams, as in other studies (Sharp et al, 1980; Klumpar and Heikkila, 1980; Collin et al, 1982) , are associated with ion conics. The association of these beams with electrostatic hiss is established in another related paper (Lin et al, 1983).

The High Altitude Plasma Instrument (HAPI) on Dynamics Explorer 1 (DE-1) made differential flux measurements of electrons and positive ions over an energy/charge range of 5 eV/e to 31 keV/e. Details of the instrument and its various operating modes can be found in Burch et al (1981). For the first few months after launch the 4.7  $R_E$  apogee of DE-1 was just poleward of the pre-noon polar cusp. A common feature of the HAPI plasma data acquired during this time period is the appearance of upward-travelling electron beams with energies from a few tens of eV to a few hundred eV. Although both upward and downward electron beams are observed in and near the cusp region, we have consistently observed a region of predominantly upward beams that overlaps the equatorward boundary of the cusp electron population.

The systematic appearance of upward electron beams near the equatorward cusp boundary, their absence in the heart of the cusp, and subsequent appearance near the cusp poleward boundary, raise the question of to what extent the electrons measured on DE-1 are charge carriers for dayside region 1 and cusp-region Birkeland currents. This question is answerable to some degree by suitable correlations between the HAPI data and data from the DE-1 magnetometer (Farthing et al, 1981). The results of the correlations for a typical pass are presented in the next section.

### B. Electron Currents and Magnetic Perturbations

The parallel (field-aligned) current density carried by a measured electron distribution  $f(v, \alpha, \phi)$  is given by

$$I_{\parallel} = e \int_0^{2\pi} \int_0^{\pi} \int_{v_{\min}}^{v_{\max}} v_{\parallel} f v v_{\perp} dv d\alpha d\phi, \quad (3)$$

where  $\alpha$  is pitch angle,  $e$  is electron charge,  $v_{\parallel}$  and  $v_{\perp}$  are the velocities parallel and perpendicular to  $\bar{B}$ ,  $v_{\min}$  and  $v_{\max}$  are the velocity limits on the measurement, and  $\phi$  is the azimuthal angle about  $\bar{B}$ . Since the electron fluxes at energies below about 15 eV are dominated by spacecraft photoelectrons, we set  $v_{\min}$  equal to the velocity of an 18 eV electron (the next energy step above 15 eV) in the current calculations. In each case,  $v_{\max}$  was set to correspond to the maximum energy sampled by the HAPI instrument.

If the spacecraft potential  $\phi_0$  is nonzero, the above calculated current is an overestimate, since the measured electron velocity is larger than the actual velocity. For the analyzer viewing perpendicular to the spin axis (therefore also normal to the spacecraft surface) the velocity  $v$  in Eq. (3) should be replaced by  $(v^2 + 2q\phi_0/m)^{1/2}$ , where  $q = -e(e)$  for electrons (ions). For a potential  $\phi_0$  of roughly 15V, and a total potential drop of 30 V (magnetospheric and spacecraft), we can overestimate the current by no more than a factor of 2.8 and most likely less.

Calculation of the electron current was performed as follows. A differential current,  $dI/dv$ , was first obtained for each energy sampled by assuming a Maxwellian distribution and applying a spline integration over  $\alpha$ . Next, the total current was obtained by integrating over  $v$  with the same technique. Ion current was also computed. However, in all cases the ion current amounted to less than 1% of the electron current.

The results of the current calculations for a cusp pass on October 6, 1981, are plotted in Figure 7, in which upward currents are plotted as positive values. Also plotted in Figure 7 are the currents determined from the magnetic perturbations ( $\delta B_\phi$ ) measured by the DE-1 magnetometer, assuming current sheets that are greatly extended in longitude and oriented perpendicular to the local dipole magnetic meridian. The agreement between the computed and measured values of the current argues strongly that electrons with energies above 15 eV are the primary charge carriers of the downward region-1 currents, the upward cusp-region currents, and another region of downward current located near the poleward boundary of the cusp in the pre-noon hours at altitudes near 20,000 km. These same three current systems, and corresponding electron populations have been observed in all four cusp passes that we have examined in detail to date.

### C. Acceleration Mechanism

Detailed study of the velocity-space distributions of the observed upward electron beams points to an acceleration region consisting of a downward field-aligned potential drop below the spacecraft. An example of the  $f(v_\parallel, v_\perp)$  distribution observed by the HAPI  $0^\circ$  analyzer on October 6, 1981, is plotted in Figure 8. To obtain optimum sampling in velocity space, Figure 8 contains  $\log_{10} f$  contours for two successive spacecraft rotations. The dots in Figure 8 identify the  $(v_\perp, v_\parallel)$  values that were sampled by the  $0^\circ$  analyzer during the two rotations. To accentuate the features of the low energy beam, Figure 8 contains data only for energies up to 500 eV.

As shown by Knight (1973), conservation of energy and of the first adiabatic invariant require that electrons originating in the ionosphere satisfy the inequality



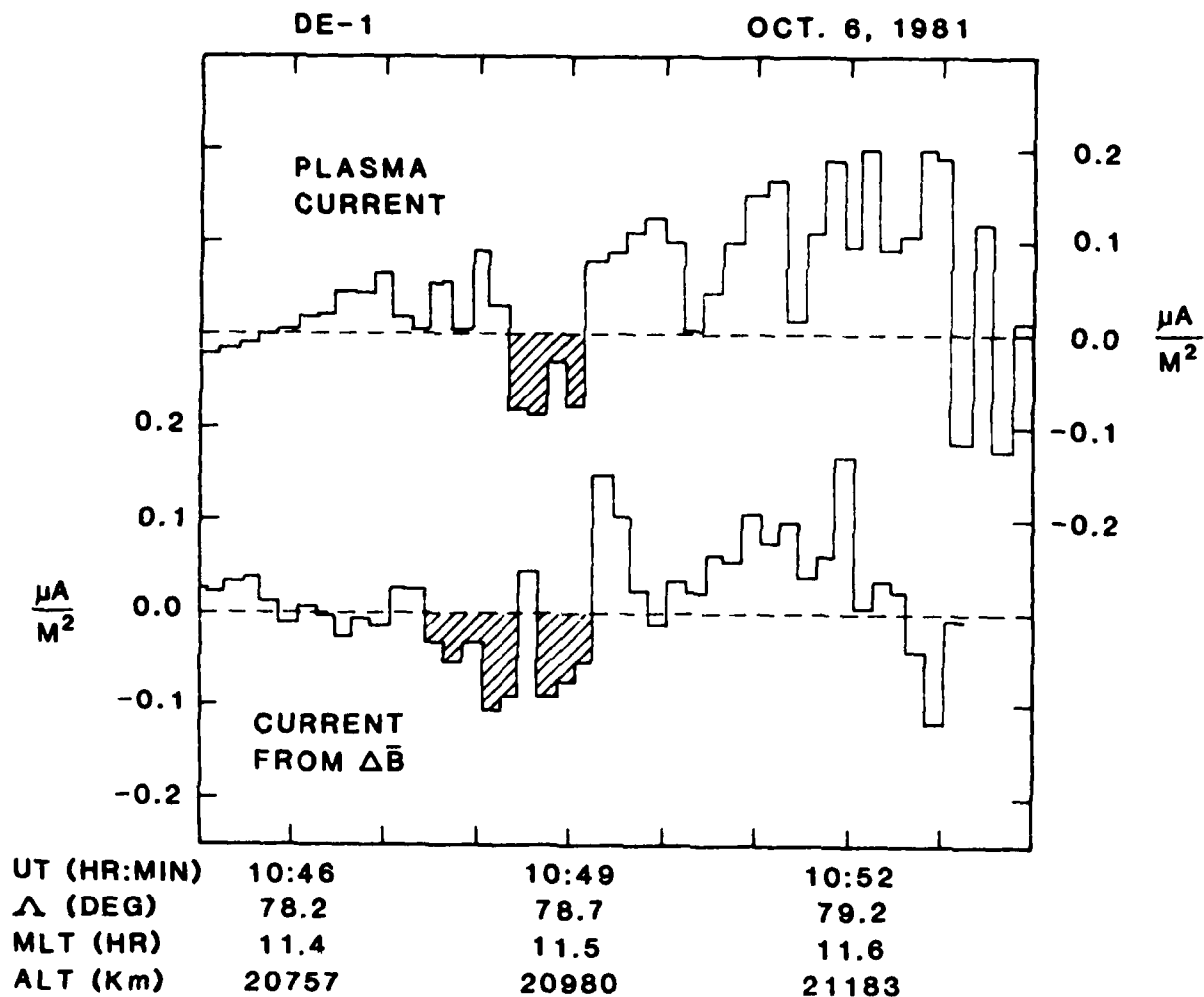


Figure 7 Field-aligned current densities computed from the measured hot-plasma distributions (top panel) and from the measured  $\Delta B$  perturbations (bottom panel). Positive currents are upward, negative currents downward. The shaded regions of downward current are identified as region-1 Birkeland currents.

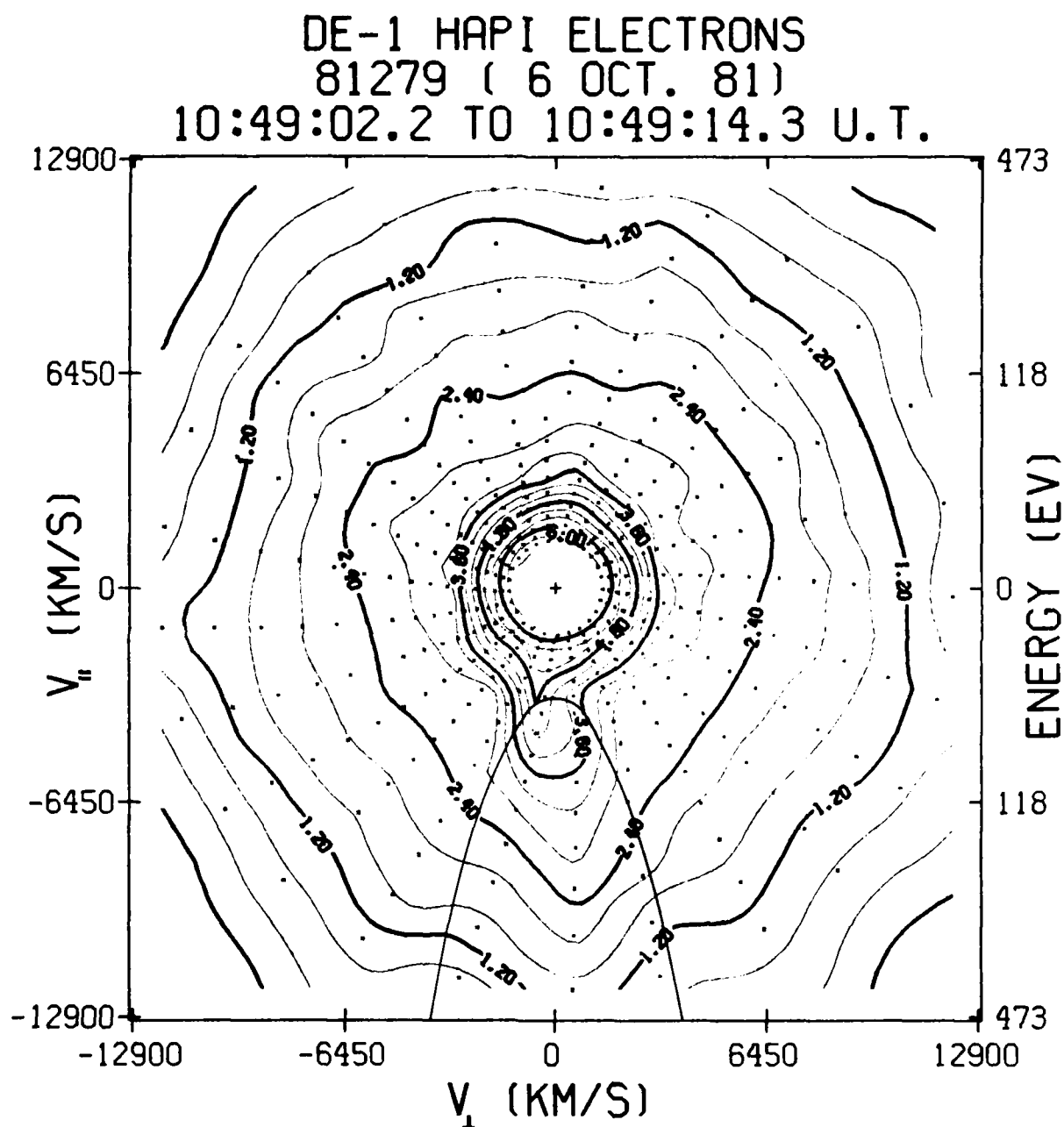


Figure 8. Electron distribution-function contours in the  $v_{\parallel}$ ,  $v_{\perp}$  plane averaged over two rotations of the DE-1 spacecraft. Also plotted is a hyperbola defined by eq. (2) for a potential drop,  $V_0 = 31$  V, with maximum altitude at 5870 km.

$$- \frac{2e}{m_e} V_0 + v_{\perp}^2 \left(1 - \frac{B_0}{B}\right) + v_{\parallel}^2 > 0, \quad (2)$$

where  $V_0$  is the electrostatic potential difference between the ionosphere and the point of observation, and  $B_0$  and  $B$  represent the magnetic induction at the top of the potential-drop region and at the point of observation, respectively. This inequality defines a region within a hyperbola with origin at (0,0) and "semi-axes"  $\sqrt{(2e/m)V_0}$  (intercept along the  $v_{\parallel}$  axis) and  $\sqrt{(2e/Am)V_0}$ , where  $A = (B_0/B) - 1$  (asymptotes  $v_{\perp} = \pm v_{\parallel}/A^{1/2}$ ). Shown in Figure 8 is such a hyperbola for a potential drop ( $V_0$ ) of 31 V extending to a maximum altitude of 5870 km. The interior of this hyperbola, or one nearly like it, does in fact define approximately the region occupied by the upward electron beam. Examination of a number of upward beams shows that these values for  $V_0$  and the altitude of the top of the potential drop region are typical. A nonzero spacecraft potential  $\phi_0$  will subtract from the inferred accelerating potential  $V_0$ .

#### D. Conclusions

Upward electron beams are observed to be a common phenomenon in regions of downward Birkeland current at altitudes above  $\sim 1 R_E$ . The electron velocity space distributions are consistent with parallel potential drops of a few tens of volts located near  $1 R_E$  altitude, or if there is a distributed potential drop instead of a double layer, the upper boundary is at about  $1 R_E$  and the lower boundary is unknown.

In the cusp region, electric current densities calculated from the measured electron distribution functions over the energy range 18 eV - 17.5 keV are in very good agreement with the current inferred from the onboard magnetometer for both downward and upward currents. Uncertainties in the orientation of the current sheet and in the spacecraft potential can readily explain the

small differences. Thus, while at lower altitudes downward currents are typically carried by near-thermal upgoing electrons (with only occasional upward beams), at altitudes above  $\sim 1 R_E$  the current is typically carried by upward beams of electrons that have been accelerated to suprathermal energies by potential drops of a few tens of eV. Computations of field-aligned currents from hot-plasma distributions observed in numerous orbits of DE-1 in both the dayside and nightside auroral zones and in the polar cap indicate that at altitudes near and above 10,000 km the majority of the current carriers are electrons within the energy range of the HAPI instrument.

## V. OBSERVATIONS OF A HEATED ELECTRON POPULATION ASSOCIATED WITH THE 6300 Å SAR ARC EMISSION

### A. Introduction and Observations

It was not until the IGY period that the existence of Stable Auroral Red (SAR) arc features was first reported (Barbier, 1958). As implied, identification of these subauroral arcs using ground-based instrumentation relies primarily on the stability and monochromatic nature of the emissions at 6300Å, a result of the 1D+3P transition of atomic oxygen.

Attention was directed toward the ring current as a potential source of energy for maintenance of the emission when early findings of Rees and Akasofu (1963) indicated a strong correlation between the presence of SAR arcs and stormtime enhanced Dst indices. Thermal conduction models, first proposed by Cole (1965), rely on the preferential excitation of atomic oxygen to the 1D state by electrons in the high energy tail of a Maxwellian distribution. High temperatures within the ionospheric electron gas are then maintained via conduction of heat along magnetic field lines threading the plasmapause-ring current region. Several mechanisms have been suggested for the actual energy transfer. These include the model of Cole (1965) which uses coulomb collisions between ring current protons and plasmaspheric electrons; that of Cornwall et al. (1971) which predicts the production of ion cyclotron wave turbulence within the ring current and its transfer to plasmaspheric electrons; and the more recent concept of Hasegawa and Mima (1978) that introduces Alfvén waves to precipitate directly low energy electrons into the SAR arc region.

Recent observations by the Dynamics Explorer-2 plasma experiment have for the first time provided measurements of the heated electrons responsible for the production of the 6300 Å SAR arc emissions. In this paper we will present data for a single SAR arc event centered at 04:05 UT on day 296 (23 October) of 1981. The event was selected for early analysis for two reasons: 1) DE-1 and DE-2 were magnetically conjugate at this time; 2) the satellite track was within the window of the Pacific Northwest Scanning Photometer (MASP) network allowing detailed comparisons between the 6300 Å SAR emission and the particle fluxes. It is in no way a unique event.

On October 23, 1981, following four days of variable SAR arc activity as monitored by the MASP network, the path of DE-2 took it over a distinct SAR arc during a period and at a location being viewed by a MASP unit located at Richland, WA ( $46.4^{\circ}\text{N}$ ,  $240.4^{\circ}\text{E}$ ). Presence of the SAR arc was confirmed by additional sightings by MASP units located near Eureka, MT and Boulder, CO. Due to weather conditions and the orbital position of DE-2, we will utilize data primarily from the Richland, WA site in this paper. A detailed description of the MASP operation is found in Kleckner et al (1981).

Fig. 9 presents contours of 6300 Å emission intensity as measured from Richland at 04:00 UT, near the time of DE-2 passage. Standard triangulation procedures with the MASP unit located near Eureka indicate a region of maximum emission at an altitude of 425-450 km. Compensation for slant path viewing of the SAR arc feature and atmospheric extinction have been applied accordingly. Also included in Fig. 9 is the DE-2 track indicated by the dashed line. The small set of circular contours near the center of the plot are artificial, serving only to locate the Richland site. The SAR arc is clearly distinguished by the band of 6300 emission lying just below  $L=3$ . Aurora poleward of the SAR arc can be seen beginning near  $L=4$ .

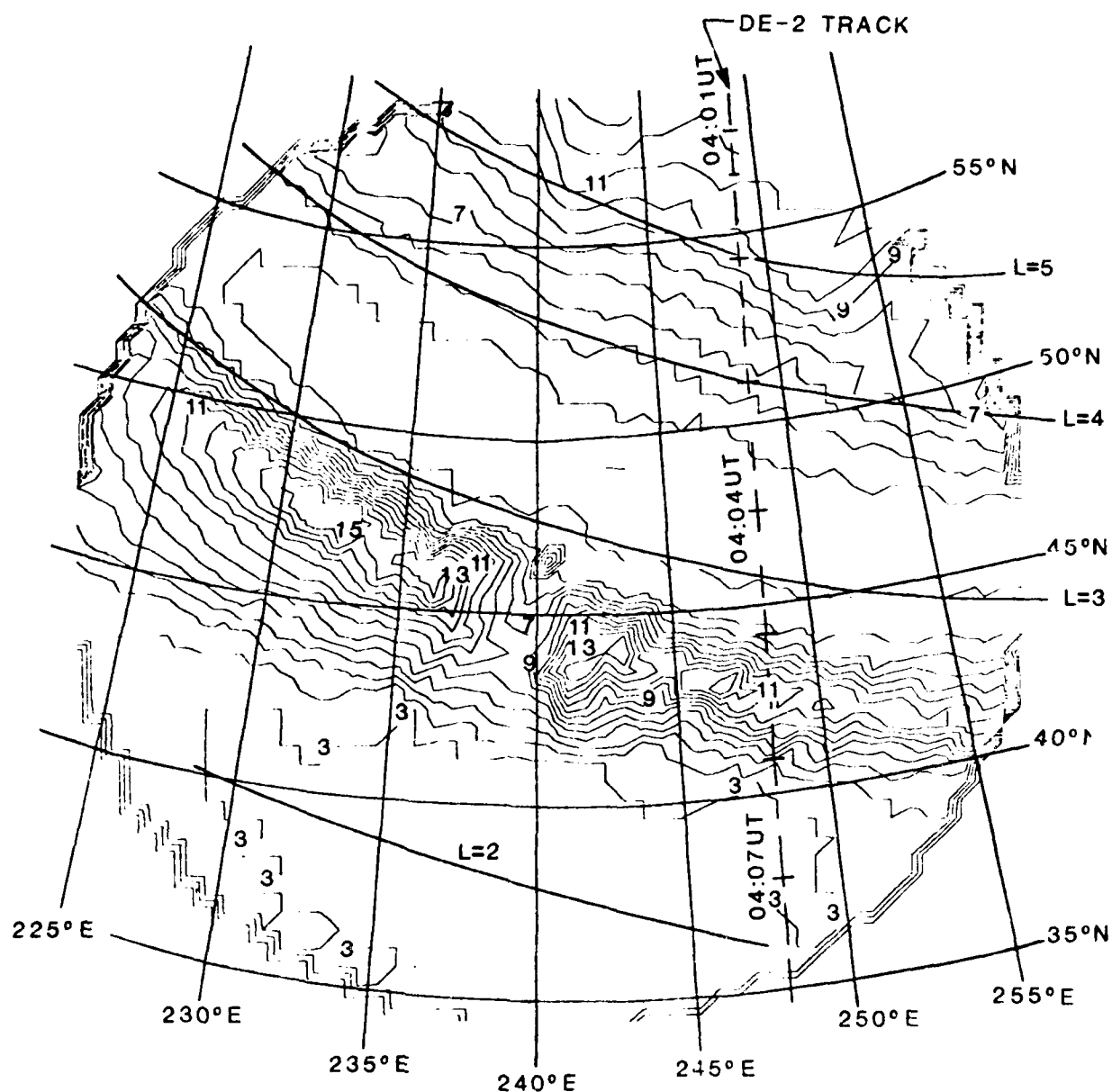


Figure 9. Contour plot of 6300Å emission as measured from Richland, WA. Contour intervals are 100 R. The path of DE-2, projected to 425 km altitude, is shown as a dashed line. The position of Richland, WA is depicted by the artificially produced contours at center of mapping.

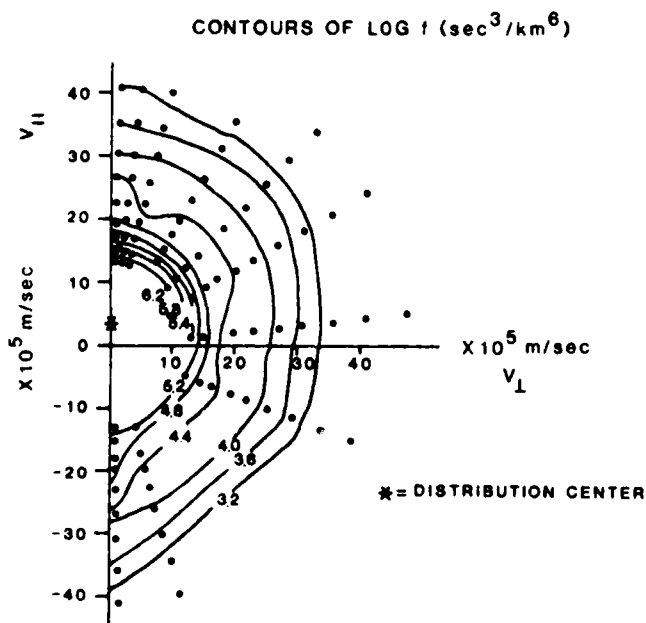
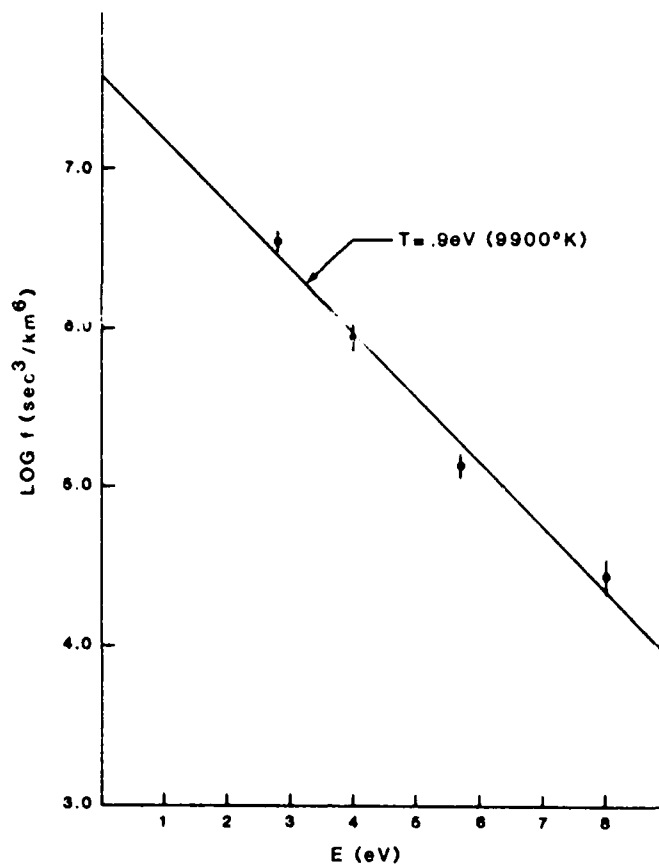
DE-1 and DE-2 were magnetically conjugate during the traversal of the SAR arc, giving a two point simultaneous plasma measurement at 850 and 6000 km. The plasma experiments on board both satellites are identical in instrumentation and response--differing only in configuration. The DE-2 plasma experiment is a family of 15 electron and 15 ion sensors mounted on a single axis, magnetically oriented scan platform allowing each detector to be held approximately fixed in pitch angle. The DE-1 plasma instrument consists of 5 electron and 5 ion detectors which scan in pitch angle with satellite rotation. A complete description of both instruments is found in Winningham et al. (1981) and Burch et al. (1981).

Many of the more important plasma features of the low energy electrons during the SAR arc can be seen in Fig. 10. The upper panel shows a typical field aligned electron distribution function plotted in the plasma rest frame. The electron population responsible for the SAR arc is located below 8 eV. The fact that the distribution can be characterized by a linear relationship in this region suggests that a Maxwellian fit to give both temperature and density may be applied. The lower panel shows the complete electron distribution function (out to 50 eV). The presence of a field aligned flow is indicated by the offset of the inner four contours. Use of the offset (about 275 km/sec in this case) allow for individual spectra to be plotted in the plasma rest frame. Calculations of both the temperature and heat flux necessitate a transformation into the plasma rest frame. Neglecting this transformation could result in significant errors.

#### B. Discussion

The identification of the low energy electron population in Fig. 10 as the particles responsible for the 6300Å SAR arc emission is based primarily





Typical field aligned electron spectrum taken near 04:05:10 UT along with the corresponding 2-D phase space contour plot. The latter distinctly shows the field aligned flow velocity of the low energy electron population.

on the correlation between the MASP photometer data and the DE-2 particle data. Fig. 11 shows the profile of the 6300Å emission along the satellite track (solid line from the Richland, WA MASP unit and dashed line from Eureka, MT unit) in Fig. 9 along with coincident particle data. The MASP data clearly show the SAR arc centered at 52°Λ. The more poleward aurora, beyond 56°Λ, is shown assuming a 300 km emission height, typical of 0(1D) emissions in the auroral zone (dashed line) and at a SAR emission height of 420 km (solid line). The particle data are shown in Fig. 11 as the log of the electron distribution function (7.5° pitch angle) at 6.7 eV (open circle), 8.8 eV (solid circle) and 20.4 eV (solid triangle). In the rest frame of the plasma the lower two energies are approximately 4.0 and 5.7 eV respectively. Changes in the 6.7 eV values can be interpreted as changes in density while changes in the 6.7-8.8 eV separation as changes in the plasma temperature. The latter, of course, assumes a Maxwellian low energy electron population and as such may not be valid outside the general SAR arc region.

The correlation between the photometer and low energy electron data is unmistakable. The distribution function at 6.7 eV tracks the 6300Å emission almost one to one. The large 6.7-8.8 eV separation within the SAR arc itself suggests a very cool electron population. Computation of the electron temperature near 52°Λ latitude (taking into account the plasma flow velocity) gives values of  $9900 \pm 110^\circ \text{ K}$ . Corresponding computations of the density using a satellite potential of  $-1.7 \pm 0.1$  volts (R. Heelis, private communication) gives a density of  $250 \pm 50 \text{ cm}^{-3}$  for this particle population.

It should be noted that there is nearly a 500 km difference between the measurement of the particles and the measurement of the 6300Å emission altitude. Some degradation of the particles in moving to the emission altitude is

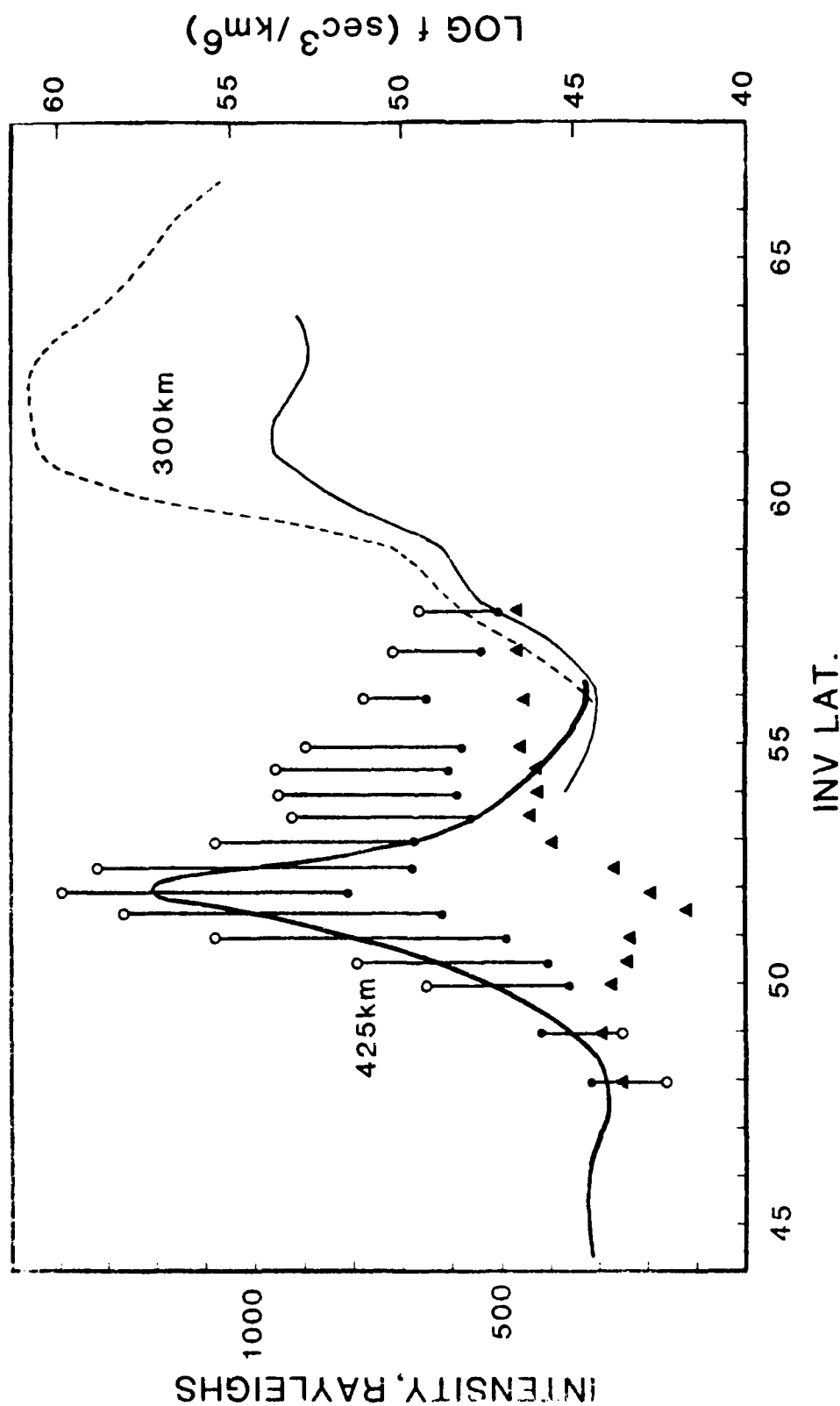


Figure 11. Profile of 6300Å emission (Rayleighs) along the DE-2 path from the Richland, WA (solid line) and Eureka, MT MASP (dashed line) units. Near 55° the emissions are computed at a height of 300 km--typical of auroral 6300Å emission. Several values of the measured distribution function are overlaid over the emission plot. Shown is the distribution function at 6.7 eV (open circles), 8.8 eV (solid circles) and 20.4 eV (solid triangles). The length of the solid line connecting the 6.8 and 8.8 eV data give an indication of the plasma temperature. The 20.4 eV data gives an indication of the photoelectron density.

expected. With a single measurement, the amount of degradation cannot be determined directly without a model. Without resorting to a specific model, however, we can make some positive statements concerning the electron transport. Between days 288 and 324 of 1981 more than 75 distinct particle populations with characteristics similar to those presented in this paper have been identified. When ground observations exist to support the satellite observations these electron populations have been found to be associated with SAR arcs. The satellite observations extend from above 900 km to 400 km which indicates the ability of this electron distribution to exist over a considerable length of the flux tube.

The day 296 SAR arc contains several features which may yield important information as to the production mechanisms responsible for the low energy electrons. In Fig. 11 one finds a decrease in the conjugate photoelectron intensity within the SAR arc. Photoelectrons give a measure of the coupling between the northern and southern hemispheres. Lee et al (1980) have postulated that such decreases might be due to enhancements in the thermal electrons within the local flux tube. This shielding phenomena has been noted in many of the SAR arc cases (both visual and subvisual) we have investigated.

There appears to be no corresponding ion precipitation accompanying the low energy electron enhancement. This is contrary to the Cornwall et al. (1971) prediction of precipitating ions on the order of  $10^8/\text{cm}^2\text{-sec}$ . This fact in conjunction with the lack of a definite low energy electron signature or enhancement during this time period, might suggest a lower altitude production for the thermal electrons. Both of these facts would seem to point to a production mechanism in line with the Hasagawa and Mima (1978) work.

### C. Summary

The low energy electrons observed by the DE-1 plasma experiment are associated with the 6300 Å SAR arc emission. The following features have been noted:

1. The heated electrons have a significant field aligned flow velocity.
2. There is no corresponding electron population observed by the DE-1 plasma instrument located at 6000 km above the SAR arc.
3. The SAR arc occurs at the plasmashet-plasmasphere overlap boundary, identified by the drop out of the plasmashet particles observed at DE-1.
4. The heated electron component appears fairly Maxwellian with temperatures of about 0.9 eV, which is not significantly different than predicted by several theories.
5. The absence of observable precipitating ring current ions within the SAR arc, which may point to mechanisms not involving ring current ions.
6. The decrease in the conjugate photoelectron intensities, indicating a partial shielding of one hemisphere from another.
7. Modeling of the energy deposition and degradation of the observed electrons should include the possibility of a continual driving source along the total flux tube.

## VI. PRESENT STATUS AND FUTURE STUDIES

Evidence presented in Section II demonstrates that processes in the high-altitude polar cusp are effective in influencing the hot plasma characteristics in the mid-and low-altitude cusp. The data set studied was small, however, and future work should be directed toward a statistical study of these processes.

The counterstreaming electron results presented in Section III demonstrate clearly that parallel electric field acceleration is important in affecting the precipitation of auroral electron fluxes. However, only a small number of such events have been studied, and the study needs to be expanded to include a more significant statistical sample of events. Special emphasis should be placed on learning the acceleration processes.

The SAR arc results cited in Section V indicate that the SAR arc emissions at mid-latitudes are produced by low-energy electron fluxes instead of ion fluxes as previously suggested. These new results need to be amplified by further comparative study.

The comparison between upward electron beams and magnetic field measurements cited in Section IV is an important step toward identification of the current carriers of the global current systems in the polar cap region. Effort should be placed on expanding this study to other local times, especially the nightside. Future emphasis should focus on study of the dynamics of these current systems.

Another fruitful area of research is the statistical characterization of plasma parameters in the polar cap region. The foundation laid down by the results cited here should facilitate this work. Preliminary results have shown that the plasma characteristics at DE-1 altitudes ( $1-4 R_E$ ) are quite distinct from those observed in the equatorial regions and above the topside ionosphere.

## REFERENCES

- Anderson, H. R., and R. R. Vondrak, Observations of Birkeland currents at auroral latitudes, Rev. Geophys. Space Phys., 13, 243, 1975.
- Anderson, H. R., Birkeland currents and auroral structure, in Auroral Processes, ed. by C. T. Russell, p. 181, Japan Scientific Societies Press, Tokyo, 1979.
- Barbier, D., The auroral activity at low altitudes, Ann Geophys, 14, 334, 1958.
- Burch, J. L., S. A. Fields, and R. A. Heelis, Polar cap electron acceleration regions, J. Geophys. Res., 84, 5863, 1979.
- Burch, J. L., P. H. Reiff, R. W. Spiro, R. A. Heelis, and S. A. Fields, Cusp region particle precipitation and ion convection for northward interplanetary magnetic field, Geophys. Res. Lett., 7, 393, 1980.
- Burch, J. L., J. D. Winningham, V. A. Blevins, N. Eaker, W. C. Gibson, and R. A. Hoffman, High Altitude Plasma Instrument for Dynamics Explorer-A, Space Sci. Instrum., 5, 455, 1981.
- Burch, J. L., P. H. Reiff, R. A. Heelis, J. D. Winningham, W. B. Hanson, C. Gurgiolo, J. D. Menietti, R. A. Hoffman, and J. N. Barfield, Plasma injection and transport in the mid-altitude polar cusp, Geophys. Res. Lett., 9, 921, 1982.
- Carlson, C. W., and R. B. Torbert, Solar wind ion injections in the morning auroral oval, J. Geophys. Res., 85, 2903, 1980.
- Chiu, Y. T., and M. Schulz, Self-consistent particle and parallel electrostatic field distributions in the magnetospheric-ionospheric auroral region, J. Geophys. Res., 83, 629, 1978.
- Cole, K. D., Stable auroral red arcs, sinks for energy of Dst main phase, J. Geophys. Res., 70, 1689, 1965.
- Collin, H. L., R. D. Sharp, and E. G. Shelley, The occurrence and characteristics of electron beams over the polar regions, J. Geophys. Res., 87, 7504, 1982.
- Cornwall, J. M., F. V. Coroniti and R. M. Thorne, Unified theory of SAR arc formation at the plasmopause, J. Geophys. Res., 76, 4428, 1971.
- Dusenbery, P. B., and L. R. Lyons, Generation of ion-conic distribution by ionospheric electrons, J. Geophys. Res., 86, 7627, 1981.

- Evans, D. S., Precipitating electron fluxes formed by a magnetic field aligned potential difference, J. Geophys. Res., 79, 2853, 1974.
- Farthing, W. H., M. Sugiura, B. G. Ledley, and L. J. Cahill, Jr., Magnetic field observations on DE-A and -B, Space Sci. Instrum., 5, 551, 1981.
- Fennell, J. F., D. J. Gorney, and P. F. Mizera, Auroral particle distribution functions and their relationship to inverted V's and auroral arcs, Physics of Auroral Arc Formation, ed. by S.-I. Akasofu and J. R. Kan, AGU, Wash. D.C., 1981, p. 91.
- Frank, L. A., Plasma in the earth's polar magnetosphere, J. Geophys. Res., 76, 5202, 1971.
- Gurgiolo, C., and J. L. Burch, DE-1 observations of the polar wind--a heated and unheated component, Geophys. Res. Lett., 9, 945, 1982.
- Gurgiolo, C., D. W. Slater, J. D. Winningham, and J. L. Burch, Observations of a heated electron population associated with the 6300Å SAR arc emission, Geophys. Res. Lett., 9, 965, 1982.
- Gurnett, D. A., and L. A. Frank, Plasma waves in the polar cusp: observations from Hawkeye 1, J. Geophys. Res., 83, 1447, 1978.
- Hanson, W. B., R. A. Heelis, R. A. Power, C. R. Lippincott, D. R. Zuccaro, B. J. Holt, L. H. Harmon, and S. Sanatani, The retarding potential analyzer for Dynamics Explorer-B, Space Sci. Instrum., 5, 503, 1981.
- Hasagawa, A., and K. Mima, Anomalous transport produced by Kinetic Alfvén wave turbulence, J. Geophys. Res., 83, 1117, 1978.
- Heelis, R. A., W. B. Hanson, C. R. Lippincott, D. R. Zuccaro, L. H. Harmon, B. J. Holt, J. E. Doherty, and R. A. Power, The ion drift meter for Dynamics Explorer-B, Space Sci. Instrum., 5, 511, 1981.
- Heikkilä, W. J., Impulsive plasma transport through the magnetopause, Geophys. Res. Lett., 9, 159, 1982.
- Iizuka, S., P. Michelson, J. J. Rasmussen, R. Schrittwieser, R. Hatakeyama, K. Saeki and N. Sato, Dynamics of a potential barrier formed on the tail of a moving double layer in a collisionless plasma, Phys. Rev. Lett., 48, 145, 1982.
- Johnstone, A. D., and J. D. Winningham, Satellite observations of suprathermal electron bursts, J. Geophys. Res., 87, 2321, 1982.
- Kleckner, E. W., J. J. Michalsky, L. L. Smith, J. R. Schmelzer, R. H. Severtsen, J. L. Berndt, and D. W. Slater, A multipurpose, computer controlled, mobile automatic scanning photometer (MASP), in Proceedings of the Finnish-American Auroral Workshop, Aug. 17-20, 1981 in Oulu, Finland, ed. L. Jalonen and T. Nygren, Finnish Academy of Science and Letters, Sodankylä Geophysical Observatory, pg. 141-148, 1981.



- Klumpar, D. M., Relationships between auroral particle distributions and magnetic field perturbations associated with field-aligned currents, J. Geophys. Res., 84, 6524, 1979.
- Klumpar, D. M., and W. J. Heikkila, Electrons in the ionospheric source cone: evidence for runaway electrons as carriers of downward Birkeland currents, Geophys. Res. Lett., 9, 873, 1982.
- Lee, J. S., J. P. Doering, T. A. Potemra, and L. H. Brace, Measurements of the ambient photoelectron spectrum from Atmosphere Explorer: II AE-E measurements from 300-100 km during solar minimum conditions, Planet. Space Sci. 28, 973, 1980.
- Lemaire, J., and M. Roth, Penetration of solar wind plasma elements into the magnetosphere, J. Atmos. Terr. Phys., 40, 331, 1978.
- Leroy, M. M., C. C. Goodrich, D. Winske, C. S. Wu and K. Papadopoulos, Simulation of a perpendicular shock, Geophys. Res. Lett., 8, 1269, 1981.
- Lin, C. S., B. Mauk, G. K. Parks, S. DeForest, and C. E. McIlwain, Temperature characteristics of electron beams and ambient particles, J. Geophys. Res., 84, 2651, 1979.
- Lin, C. S., J. L. Burch, S. D. Shawhan, and D. A. Gurnett, Correlation of electrostatic hiss and upward electron beams near the polar cusp, submitted to J. Geophys. Res., 1983.
- Maier, E. J., S. E. Kayser, J. R. Burrows, and D. M. Klumpar, The suprathermal electron contributions to high-latitude Birkeland currents, J. Geophys. Res., 85, 2003, 1980.
- Mizera, P. F., J. F. Fennell, D. R. Croley, Jr., and D. J. Gorney, Charged particle distributions and electric field measurements from S3-3, J. Geophys. Res., 86, 7566, 1981.
- Moore, T. E., and R. L. Arnoldy, Plasma pitch angle distributions near the substorm injection front, J. Geophys. Res., 87, 265, 1982.
- Rees, M. H., and S. Akasofu, On the association between subvisual red arcs and the Dst(H) decrease, Planet. Space Sci., 11, 105, 1963.
- Reiff, P. H., T. W. Hill, and J. L. Burch, Solar wind plasma injection at the dayside magnetospheric cusp, J. Geophys. Res., 82, 479, 1977.

- Reiff, P. H., J. L. Burch, and R. W. Spiro, Cusp proton signatures and the interplanetary magnetic field, J. Geophys. Res., 85, 5997, 1980.
- Russell, C. T., and E. W. Greenstadt, Initial ISEE magnetometer results; shock observations, Space Sci. Rev., 23, 3, 1979.
- Sharp, R. D., R. G. Johnson, and E. G. Shelley, Energetic particle measurements from within ionospheric structures responsible for auroral acceleration processes, J. Geophys. Res., 84, 480, 1979.
- Sharp, R. D., E. G. Shelley, R. G. Johnson, and A. G. Ghielmetti, Counter streaming electron beams at altitudes of  $\approx 1 R_E$  over the auroral zone, J. Geophys. Res., 85, 92, 1980.
- Shelley, E. G., R. D. Sharp, and R. G. Johnson, He<sup>++</sup> and H<sup>+</sup> flux measurements in the dayside cusp: estimates of convection electric field, J. Geophys. Res., 81, 2363, 1976.
- Wagner, J. S., A computer simulation of auroral arc formation, Ph.D. thesis, Geophysics Institute, Univ. of Alaska, Fairbanks, Alaska, 1980.
- Wagner, J. S., J. R. Kan, S.-I. Akasofu, T. Tajima, J. N. Leboeuf and J. M. Dawson, A simulation study of V-potential double layers and auroral arc formations, Physics of Auroral Arc Formation, ed. by S.-I. Akasofu and J. R. Kan, AGU, Washington, D.C., 1981, p. 304.
- Winningham, J. D., J. L. Burch, N. Eaker, V. A. Blevins and R. A. Hoffman, the low altitude plasma instrument (LAPI), Space Sci. Instrument., 5, 465, 1981.
- Winningham, J. D., and C. Gurgiolo, DE-2 photoelectron observation consistent with a large scale parallel electric field over the polar cap, Geophys. Res. Lett., (this issue).
- Zanetti, L. J., T. A. Potemra, J. P. Doering, J. S. Lee, and R. A. Hoffman, Magnetic field-aligned electron distributions in the dayside cusp, J. Geophys. Res., 86, 8957, 1981.

## PAPERS PRESENTED AT SCIENTIFIC MEETINGS

Edwards, P.A., L.A. Frank, J.D. Craven, J.L. Burch and J.D. Winningham,

Sun-aligned polar cap auroral arcs and their implications concerning magnetospheric dynamics, paper presented at the spring annual meeting of the American Geophysical Union, May, 1982

Varosi, F., H.G. Mayr, H.S. Porter, L.A. Frank, J.D. Craven, J.D. Winningham,

L.H. Brace, Precipitating electron distribution inferred from dynamics explorer (DE-1) auroral images, paper presented at the spring annual meeting of the American Geophysical Union, May, 1982

Burch, J.L., J.D. Winningham and C. Gurgiolo, Simultaneous hot plasma

observations by dynamics Explorer 1 and 2, paper presented at the spring annual meeting of the American Geophysical Union, May, 1982

Lin, C.S., J.L. Burch, J.D. Menietti and J.D. Winningham, DE observations of

counterstreaming electrons: a HAPI look, paper presented at the spring annual meeting of the American Geophysical Union, May, 1982

Kozyra, J.U., T.E. Cravens, A.F. Nagy, L.H. Brace, N.C. Maynard, J.D. Winningham

and B.A. Emery, Observational characteristics of stable auroral red arc events, paper presented at the spring annual meeting of the American Geophysical Union, May, 1982

Hernandez, G., J.W. Meriether, D.W. Slater, R.G. Roble, B.A. Emery, J.U. Kozyra,

A.F. Nagy, L.H. Brace, J.D. Winningham, and D.S. Evans, Thermospheric response to the October 21 and 23, 1981 SAR-arcs and aurora as observed from Fritz Peak, Colorado, and Calgary, Alberta during the Dynamics Explorer (DE-2) and NOAA-6 satellite overflights, paper presented at the spring annual meeting of the American Geophysical Union, May, 1982

Curtis, S.A., W.R. Hoegy, L.H. Brace, N.C. Maynard, M. Sugiura and D. Winningham,  
Ionospheric temperature and density structuring in the low altitude  
polar cusp, paper presented at the spring annual meeting of the  
American Geophysical Union, May, 1982

Chang, Tom, B. Coppi, J. Jasperse, B. Basu, and J. Retterer and J.L. Burch,  
Electron beams, lower hybrid waves, and ion conics in the lower  
supraauroral region, paper presented at the spring annual meeting of  
the American Geophysical Union, May, 1982

Sharber, J.R., J.D. Winningham and E.J. Weber, Comparison of DE-2 soft particle  
observations with 6300A enhancements in the polar cap, paper  
presented at the fall annual meeting of the American Geophysical  
Union, December, 1982

Slater, D.W., C. Gurgiolo, E.W. Kleckner, J.D. Winningham and J.L. Burch,  
Observational evidence of a SAR-arc energy source: precipitating  
electrons, paper presented at the fall annual meeting of the American  
Geophysical Union, December, 1982

Lin, C.S., J.L. Burch, D.A. Gurnett and S.D. Shawhan, Plasma instabilities  
equatorward of the polar cusp, paper presented at the fall annual  
meeting of the American Geophysical Union, December, 1982

Heelis, R.A., J.D. Winningham, D.M. Klumpar, M. Sugiura, N.C. Maynard and  
L.H. Brace, DE-2 observations of transverse and parallel ion  
acceleration, paper presented at the fall annual meeting of the  
American Geophysical Union, December, 1982

Burch, J.L. and P.H. Reiff, Upward electron beams measured by DE-1 - a potential  
source of dayside region-1 field-aligned currents, paper presented at  
the fall annual meeting of the American Geophysical Union,  
December, 1982

## PUBLICATIONS SUPPORTED BY CONTRACT

Burch, J. L., P. H. Reiff, R. A. Heelis, J. D. Winningham, W. B. Hanson, C. Gurgiolo, J. D. Menietti, R. A. Hoffman, and J. N. Barfield, Plasma injection and transport in the mid-altitude polar cusp, Geophys. Res. Lett. 9, 921, 1982.

Gurgiolo, C., and J. L. Burch, DE-1 observations of the polar wind--a heated and unheated component, Geophys. Res. Lett., 9, 945, 1982.

Gurgiolo, C., D. W. Slater, J. D. Winningham, and J. L. Burch, Observations of a heated electron population associated with the 6300Å SAR arc emission, Geophys. Res. Lett., 9, 965, 1982.

Lin, C. S., J. L. Burch, S. D. Shawhan, and D. A. Gurnett, Correlation of electrostatic hiss and upward electron beams near the polar cusp, submitted to J. Geophys. Res., 1983.

Winningham, J. D., and C. Gurgiolo, DE-2 photoelectron observation consistent with a large scale parallel electric field over the polar cap, Geophys. Res. Lett., 9, 977, 1982.

## PERSONNEL

The following persons contributed to the work reported:

J.N.Barfield, principal investigator  
C.S.Lin  
J.L.Burch  
J.D.Winningham  
C.Gurgiolo  
J.D.Mennietti  
R.W.Janetzke  
MC.Stein  
J.Davis  
K.Birkelbach

END

FILMED

9-83

DTIC